HHS Public Access

Author manuscript

NanoImpact. Author manuscript; available in PMC 2021 April 01.

Published in final edited form as:

NanoImpact. 2020 April ; 18: . doi:10.1016/j.impact.2020.100214.

Toxicity assessment of metal oxide nanomaterials using *in vitro* screening and murine acute inhalation studies

Sudartip Areecheewakul[a,1], **Andrea Adamcakova-Dodd**[b,1], **Brittany E. Givens**[a], **Benjamin R. Steines**[b], **Yifang Wang**[c], **David K. Meyerholz**[d], **Nathanial J. Parizek**[c], **Ralph Altmaier**[b], **Ezazul Haque**[c], **Patrick T. O'Shaughnessy**[b], **Aliasger K. Salem**[a,*], **Peter S. Thorne**[b,c,**]

[a]Department of Pharmaceutical Sciences and Experimental Therapeutics, University of Iowa, Iowa City, IA 52246, USA

[b]Department of Occupational and Environmental Health, University of Iowa, Iowa City, IA 52246, USA

[c]Interdisciplinary Graduate Program in Human Toxicology, University of Iowa, Iowa City, IA 52246, USA

[d]Department of Pathology, University of Iowa, Iowa City, IA 52246, USA

Abstract

Characterizations and *in vitro* toxicity screening were performed on metal oxide engineered nanomaterials (ENMs) independently comprising ZnO, CuO, CeO_2, Fe_2O_3, WO_3, V_2O_5, TiO_2, Al_2O_3 and MgO. Nanomaterials that exhibited the highest toxicity responses in the *in vitro* screening assays (ZnO, CuO, and V_2O_5) and the lesser explored material WO_3 were tested for acute pulmonary toxicity *in vivo*. Female and male mice (C57Bl/6J) were exposed to aerosolized metal oxide ENMs in a nose-only exposure system and toxicity outcomes (biomarkers of cytotoxicity, immunotoxicity, inflammation, and lung histopathology) at 4 and 24 h after the start of exposure were assessed. The studies were performed as part of the NIEHS Nanomaterials Health Implications Research consortium with the purpose of investigating the effects of ENMs on various biological systems. ENMs were supplied by the Engineered Nanomaterials Resource and Coordination Core. Among the ENMs studied, the highest toxicity was observed for CuO and ZnO

*Corresponding author. **Correspondence to: P.S. Thorne, Department of Occupational and Environmental Health, The University of Iowa, College of Public Health, 145 N. Riverside Dr., S341A CPHB, Iowa City, IA 52242, USA. aliasger-salem@uiowa.edu (A.K. Salem), peter-thorne@uiowa.edu (P.S. Thorne).

[1]Joint first authors.

CRediT authorship contribution statement

Sudartip Areecheewakul: Methodology, Formal analysis, Investigation, Writing - original draft, Writing - review & editing. **Andrea Adamcakova-Dodd:** Conceptualization, Methodology, Formal analysis, Investigation, Writing - original draft, Writing - review & editing, Supervision, Project administration, Funding acquisition. **Brittany E. Givens:** Methodology, Investigation, Writing - original draft. **Benjamin R. Steines:** Investigation. **Yifang Wang:** Investigation. **David K. Meyerholz:** Investigation. **Nathanial J. Parizek:** Formal analysis, Investigation. **Ralph Altmaier:** Investigation. **Ezazul Haque:** Methodology, Formal analysis, Investigation, Writing - review & editing. **Patrick T. O'Shaughnessy:** Conceptualization, Methodology, Funding acquisition. **Aliasger K. Salem:** Conceptualization, Writing - review & editing, Supervision, Funding acquisition. **Peter S. Thorne:** Conceptualization, Methodology, Writing - review & editing, Supervision, Project administration, Funding acquisition.

Declaration of competing interest

The authors declare that they have no known competing financial interests or personal relationships that could have appeared to influence the work reported in this paper.

Appendix A. Supplementary data

Supplementary data to this article can be found online at https://doi.org/10.1016/j.impact.2020.100214.

NPs in both *in vitro* and *in vivo* acute models. Compared to sham-exposed controls, there was a significant increase in bronchoalveolar lavage neutrophils and proinflammatory cytokines and a loss of macrophage viability at both 4 h and 24 h for ZnO and CuO but not seen for V_2O_5 or WO_3. These effects were observed in both female and male mice. The cell viability performed after *in vitro* exposure to ENMs and assessment of lung inflammation after acute inhalation exposure *in vivo* were shown to be sensitive endpoints to predict ENM acute toxicity.

Keywords

Nanomaterials; Nanoparticles; *In vitro* toxicity; Inhalation toxicity; Metal oxides

1. Introduction

Nanomaterials have gained a significant amount of attention due to their unique properties distinguishing them from their bulk counterparts. In particular, nanomaterials have high surface area to volume ratios as a result of their small size; this increases the activity of many particles and elicits novel properties including varied optical, electrical, catalytic, and magnetic functionalities (Navrotsky, 2001; Lai et al., 2018; Louro et al., 2019). Nanomaterials occur in the environment as products of combustion (Holder et al., 2012) and are manufactured intentionally to achieve specific properties such as with engineered nanomaterials (ENMs). In the studies we report here, the focus of toxicity assessment was on metal oxide ENMs.

Metal oxide ENMs have common uses in a variety of applications including biomedical therapeutics, medical implants, bio-imaging, biosensing, and in the manufacture of cosmetics, pigments and electronic devices (Andreescu et al., 2012; Chavali and Nikolova, 2019). With their increased use in both consumer products and industrial processes, concern surrounding the toxicity of these materials is of increasing importance. This is especially the case for inhalable ENMs since pulmonary exposure is one of the most frequent unintentional routes of exposure (Ahamed et al., 2015). The toxicity of some ENMs (TiO_2, ZnO, CuO, CeO_2, and Fe_2O_3) has been extensively studied both *in vitro* and *in vivo* after inhalation exposure (Grassian et al., 2007; Adamcakova-Dodd et al., 2014; Pettibone et al., 2008; Schwotzer et al., 2017). However, there are limited toxicological data on other ENMs that have become commercially important more recently such as V_2O_5 and WO_3. The toxicity of vanadium oxide NMs with different oxidation forms (V_2O_5, V_2O_3, or VO_2) on the pulmonary system either *in vitro* or *in vivo* has received some attention (Worle-Knirsch et al., 2007; Kulkarni et al., 2014) but studies of WO_3 nanoparticles (NPs) are limited (Prajapati et al., 2017).

The studies reported herein were performed as part of the NIEHS Nanomaterials Health Implications Research (NHIR) consortium with the purpose of investigating the effects of ENMs on various biological systems. The metal oxide ENMs used for our studies were chosen based on their abundance in a variety of applications (Golbamaki et al., 2015) as well as on an agreement of all NHIR Consortium members. All materials provided and characterized by the Engineered Nanomaterials Resource and Coordination Core (ERCC)

were produced by either flame spray pyrolysis (FSP), a technique for cost-effective and scalable synthesis of nanomaterials that is used in the industry (Gröhn et al., 2014; Teoh et al., 2010), or were purchased from commercial sources (Supplementary Table 1). *In vivo* studies examining the toxicity of ENMs generally provide more meaningful data than *in vitro* studies, however, they are costly and time consuming especially when a large number of ENMs need to be evaluated (Bakand et al., 2005). Cost-effective *in vitro* approaches have significant potential for primary toxicity screening of metal oxide ENMs. Pal et al. assessed the toxicity of eight ENMs *in vitro* in human monocyte/macrophage (THP-1) cells (Pal et al., 2015). Liu et al. investigated the toxicity of seven metal oxide ENMs in RAW 264.7 murine macrophages and Beas-2B human bronchial epithelial cells (Liu et al., 2015). Rat alveolar macrophages were used in *in vitro* assay predicting the short-term inhalation toxicity of nanomaterials (Wiemann et al., 2016). Previous attempts at assessing the potential harmful effects of a wide range of ENMs have been made, however, it is difficult to collect and compare the data acquired by independent laboratories because of differences in experimental factors and techniques. Differences in nanomaterial dispersion techniques, cytotoxicity assays, cell lines, and the ENM properties themselves could affect the results of *in vitro* cytotoxicity assessments. A standard protocol for preparation and characterization on ENMs was developed by Deloid et al. to ensure consistent and reliable results between *in vitro* toxicity experiments of the same ENMs at different times and/or laboratories (DeLoid et al., 2017a). This protocol for ENM dispersion was applied in this study to minimize the variation between replicated experiments and to enable comparisons with other laboratories using the same protocol.

A cytotoxicity assay was conducted investigating several ENMs provided by the ERCC to screen the materials for their potential toxicities. Those ENMs exhibiting toxicity were further evaluated for cytotoxicity, immunotoxicity, and pulmonary inflammation in an acute exposure murine model established in our laboratory (Grassian et al., 2007; Adamcakova-Dodd et al., 2014; Pettibone et al., 2008), in both females and males. ENM concentrations used in the *in vitro* studies were determined based on common concentrations used in the literature and also the calculated doses per surface area of exposed cells that were equivalent to estimated doses deposited in the pulmonary region (alveolar surface area) in acute inhalation exposures in mice.

The aim of our studies was to establish a screening method for toxicity of inhaled ENMs using *in vitro* and *in vivo* acute protocols. In particular, we investigated if simple endpoints such as cell viability (after exposure to ENMs at *in vitro* submersed conditions) and lung inflammation (after acute inhalation exposure of mice) can serve as sensitive endpoints for toxicity prediction. The cytotoxicity of nine metal oxide ENMs (ZnO, CuO, CeO_2, Fe_2O_3, WO_3, V_2O_5, TiO_2, Al_2O_3 and MgO) was assessed using the human alveolar lung adenocarcinoma cell line, A459. Those ENMs demonstrating toxicity *in vitro* (ZnO, CuO, and V_2O_5) and the novel ENM, WO_3, were further investigated using an *in vivo* nose-only acute exposure model.

2. Materials and methods

2.1. Dispersion and characterization of ENMs for in vitro studies

All ENMs used in this study were provided and characterized by the NHIR ERCC (Supplementary Table 1) (DeLoid et al., 2017a; Lee et al., 2018; Zhang et al., 2019; Beltran-Huarac et al., 2018; Zimmerman et al., 2019; Stueckle et al., 2017; Cohen et al., 2018; DeLoid et al., 2017b). The dispersion protocol of DeLoid et al. (2017a) was followed. Stock ENM suspensions (0.5 mg/mL) were prepared using 2 mg ENMs and 4 mL distilled water and vortexed for 30 s. The stock suspensions were then sonicated in a cup horn sonicator (QSonica, CT) at 75% amplitude for the necessary time to reach the critical delivered sonication energy (DSE_{cr}) specified by the ERCC (Supplementary Table 1). To maintain suspension homogeneity during the sonication, the suspension was sonicated with additional vortexing at specific time intervals as shown in Supplementary Table 1. The 20 nm MgO ENMs were prepared differently from other ENMs because MgO is highly reactive in water forming magnesium hydroxide (MgOH). Therefore, the MgO ENMs were dispersed in serum-containing media at a concentration of 0.5 mg/mL and vortexed for 30 s. The stock ENM suspensions were diluted to the concentrations of 0.03, 5.0, 50, and 100 μg/mL for MTS assay and 0.045, 7.5, 75, and 150 μg/mL for viable cell count using either serum-free media (SFM) or serum-containing media (SCM) and vortexed for 30 s prior to dosing in the *in vitro* cytotoxicity assay. The SFM was prepared from RPMI-1640 (Gibco) supplemented with 1% (v/v) 1 M HEPES buffer solution (Gibco), 1% (v/v) 100× glutaMAX™-I (Gibco), 1% (v/v) 100 mM sodium pyruvate (Gibco), and 0.1% (v/v) 50 mg/mL gentamicin sulfate (Gibco). The SCM was prepared using RPMI-1640 and all the aforementioned supplements along with 10% (v/v) fetal bovine serum (FBS, Atlanta Biologicals). The agglomeration behavior of ENMs in solution was determined by measuring the hydrodynamic diameter using a Zetasizer NanoZS (Malvern instrument Ltd., Westborough, MA) immediately after ENM preparation and 24 h after storage at 37 °C in either SFM or SCM at a concentration of 0.1 mg/mL, which was the highest concentration used in MTS cytotoxicity testing. The samples measured after 24-h preparation were incubated at 37 °C to match cell culture conditions to study whether the form agglomerates were stable over cell incubation time.

2.2. In vitro cytotoxicity using MTS assay

A549 cells (ATCC) were maintained in SCM in T75 culture flasks, and all studies were conducted between passage numbers 12–24. A549 cells were seeded at 1×10^5 cells/mL in a 96-well plate (100 μL/well) in SCM and allowed to grow overnight. The cells were checked under a light microscope and if the wells were at least 50% confluent, we proceeded with the experiment. The medium was removed, and 100 μL ENMs in either SFM or SCM at 0.03, 5, 50, or 100 μg/mL were added to each well and allowed to incubate for either 4 or 24 h. The 4-h incubation was selected to match the amount of time that the mice were exposed to the ENMs in the *in vivo* study while the 24-h incubation was used in accordance with the literature. After the designated time, cells were washed twice with DPBS (Gibco) and 100 μL of fresh SFM was added to each well. After this, 20 μL of MTS tetrazolium compound (CellTiter 96® AQueous One Solution, Promega, Madison, WI) was added and allowed to incubate at 37 °C for up to 4 h. Then, 90 μL of supernatant from each well was transferred to a new 96-well plate to avoid interference from absorbance properties of ENMs. The

absorbance of the transformed compound was measured at 490 nm and each sample was compared to the untreated control group to obtain the relative viability.

2.3. In vitro cytotoxicity using viable cell count with propidium iodide (PI) staining

A549 cells (ATCC) were seeded at a density of 1×10^5 cell/mL (2 mL SCM/well) into a 6-well plate and incubated for 24 h. The cells were checked under a light microscope and if the wells were at least 50% confluent, we proceeded with the experiment. The medium was removed and then the cells were treated with 2 mL ENMs in either SFM or SCM added to each well at 0.045, 7.5, 75, and 150 μg/mL. These concentrations are equivalent to the ones used in MTS assay study (0.03, 5, 50, and 100 μg/mL, respectively) based on mass per surface area of well. The cells were treated for either 4 or 24 h before counting the viable cell number. At the end of the incubation time, the cells were washed twice with 1× DPBS (Gibco) and trypsinized with 1 mL trypsin-EDTA (0.25%) (Gibco) for 5 min. The trypsinized cells were added with 4 mL SCM and centrifuged at 230*g* for 5 min to collect the cell pellet. The pellet was suspended in 0.5 mL SCM. The number of viable cells in each sample was determined using an automated cell counter (Moxi GO II, Orflo technologies, LLC, Ketchum, ID) with PI staining.

2.4. Delivered-to-cell dose of ENMs

In this study, dose delivered to cells data were provided by NHIR ERCC (Table 1). The dose delivered to cells for all ENMs suspended in SCM was determined using the protocol by DeLoid et al. (2017a). This protocol used a distort grid model with two key input parameters, effective density and volume weighted size distribution, which were material and media specific.

2.5. Acute in vivo toxicity

Male and female C57BL/6J mice (4- and 5-wk old at arrival, respectively) from Jackson Laboratories (Bar Harbor, ME) were utilized in these studies. Females were 1 wk older to facilitate a better fit in nose-only holders of the exposure system because of their smaller size than males. All animals were housed in an AAALAC-accredited vivarium, in polypropylene, fiber-covered cages in HEPA-filtered Thoren caging units (Hazelton, PA). Animals were acclimatized for 7 days after their arrival and were maintained in the vivarium with a 12-h light/dark cycle with *ad libitum* access to food and water. All protocols performed were approved by the University of Iowa Institutional Animal Care and Use Committee. Animal handling and exposures conformed to the NIH Guide for the Care and Use of Laboratory Animals.

Selected ENMs were evaluated for their toxicity using an acute exposure protocol with inhalation exposure lasting 4 h and necropsy after the exposure (4 h time point) or 24 h after the start of the exposure (24 h time point). Each ENM was investigated in its own exposure study. Animals (females and males) were exposed to atmospheres of particle laden-aerosol in the nose-only inExpose System (SCIREQ Inc., Emka Technologies, Montreal, Canada). Mice were acclimated to the nose-only holders one day prior the exposure to minimize stress and were not anesthetized during the exposures. The target concentration for all exposures was 3.5 mg/m^3; Table 2 lists measured exposure concentrations used for each tested ENMs.

Shams (control animals) were exposed to HEPA-filtered laboratory air in the identical nose-only system in an adjacent laboratory dedicated to sham exposures. Euthanasia of mice was performed with an overdose of isoflurane followed by cervical dislocation, thoracotomy and exsanguination through the heart.

ENM-laden aerosol was generated from a suspension of NPs in water (Optima LC/MS grade, Fisher Scientific, Pittsburgh, PA) using a 6-jet Collison nebulizer (Mesa Labs, Butler NJ) (Fig. 1). Particle suspensions were sonicated in a cup horn sonicator (QSonica, Newtown CT) for 5 min. Table 2 lists the concentrations of NP suspensions that were used in the nebulizer. To prevent particle settling during nebulization, a magnetic stir bar was placed into the nebulizer and the nebulizer was positioned on a stir plate. Dehumidified and HEPA-filtered air was supplied to the nebulizer at 1.4 bar. Generated particle-laden aerosol from the nebulizer passed through a brass drying column heated to 110 °C and a particle neutralizer (Model 3012, TSI Inc., Shoreview, MN) prior to entering two nose-only inExpose towers. Mass exposure concentration of generated aerosol was determined using a photometric method with the use of an aerosol photometer (pDR, personal DataRAM™ pDR-1500, ThermoFisher Scientific, Waltham, MA), and a gravimetric method with the use of glass fiber filters (37 mm in diameter, Whatman, Middlesex, UK) located on the exhaust side of the pDR. An internal pump within the pDR sampled the air directly from one of the nose-only ports at 2 L/min. The filters were changed every 1 or 2 h. A stainless steel sampler holding 47-mm glass fiber filter was placed on the bottom of each nose-only tower to minimize particulate release into the hood. All filters were pre- and post-weighed in a dedicated climate-controlled room using a six-place microbalance (XP26, Mettler Toledo, Mettler-Toledo, Inc., Columbus, OH). A scanning mobility particle sizer (SMPS, Model 3938, TSI Inc.), with an aerosol neutralizer (Model 3088, TSI Inc.) and a standard differential mobility analyzer (Model 3081 L, TSI, Inc.), was used to determine the particle size distribution of generated aerosol sampled from the nose-only port on the inExpose tower. Geometric mean (GM) mobility diameter and geometric standard deviation (GSD) of aerosol sizes in individual exposures were obtained from software supplied by the vendor (Table 2).

2.5.1. Estimated dose—The estimated deposited doses in the pulmonary region for each ENM used in these studies ranged between 3 and 5 μg/mouse (4–7 ng/cm^2) and are reported in Table 3. The dose calculation assumed a minute volume of 25 mL/min. The pulmonary deposition fraction for each ENM was calculated using the computational Multiple-Path Particle Dosimetry (MPPD) model (software version 3.04, available at: https://www.ara.com/products/multiple-path-particle-dosimetry-model-mppd-v-304) (Asgharian et al., 2014).

2.6. End-point toxicity measurements in vivo

Pulmonary inflammatory responses at two time points were assessed in bronchoalveolar lavage (BAL) fluid: 4 h time point (n = 5) and 24 h time point (n = 6) in both sexes. Animals were euthanized, heart exsanguination was performed and the right lobes of the lungs were lavaged 3 times with 1 mL of 0.9% sterile sodium chloride solution (Baxter, Deerfield, IL). Collected BAL fluid was centrifuged at 800*g* for 5 min at 4 °C; supernatants were frozen at

−80 °C for later determination of total protein and cytokines/chemokines. Cell pellets were resuspended in 200 μL Hank's balanced salt solution (Life Technologies, Grand Island, NY). Cell viability (with PI stianing) and total cell counts were performed using MFS cassettes (MXC020) and an automated cell counter (Moxi GO II, Orflo Technologies, LLC, Ketchum, ID). The total cell counts and viability measurements were performed at two size ranges: 9.5 and 21.5 μm (representing mainly the diameter of monocytes/macrophages and large lymphocytes) and 6.5–23 μm (including neutrophils and eosinophils). For determination of differential cell counts (number of macrophages, neutrophils, lymphocytes, and eosinophils) cells were fixed on glass microscope slides with fetal calf serum (Cytospin 4, Thermo Shandon, Thermo Scientific, Waltham, MA) and stained using Protocol® HEMA 3 stain set (Fisher Diagnostics, Pittsburgh, PA). A total of 400 cells were evaluated to differentiate the cells by type using an optical microscope (Olympus, Center Valley, PA).

The number of samples evaluated for the cytokine and total protein concentrations in BAL fluid, as well as histopathology evaluation for each experimental group and time point was determined based on the inflammatory responses seen in the BAL fluid. We evaluated 10 lung tissues for each time point for CuO and ZnO and 2 lung tissues for each time point for V_2O_5 and WO_3, representing both male and female mice. For statistical comparison of cytokine concentrations between experimental groups and shams, all values measured in shams were grouped together.

Cytokines/chemokines in BAL fluid supernatants (MIP-1a, KC, IL-10, IL-12p40, IL-6, MCP-1, G-CSF) were determined using a multiplex magnetic bead assay (Milliplex MAP kit, selected cytokines from MCYTOMAG-70K (EMD Millipore Corporation) and read on Luminex 100, Bio-Rad Laboratories, Inc., Hercules, CA). Total protein was determined using Quick Start Bradford Dye Reagent (Bio-Rad Laboratories).

After BAL collection, right lobes of the lungs were first perfused with 10% buffered formalin (Fisher Scientific, Kalamazoo, MI) through cannulated trachea and then stored in 10% buffered formalin until further processing. Tissues were then paraffin-embedded, sectioned (5-μm thickness) and stained with hematoxylin and eosin (H&E). Lung tissues were evaluated for key histopathologic changes including increased and activated number of macrophages and granulocytes, perivascular cuffing (infiltration of leukocytes around vessels), alveolar injury (evidenced by sloughing/cellular debris in alveolar lumen), reactive pneumocytes (hyperplastic/proliferative cells), necrosis (presence of cellular debris or overt necrosis of airway epithelia) and edema (eosinophilic fluid within airspaces). All lung tissues were evaluated by the board-certified veterinary pathologist using the post-examination masking method and following principles of reproducible tissue scoring (Meyerholz and Beck, 2018; Meyerholz et al., 2018).

2.7. In vivo dosimetry analyses using microwave assisted acid digestion and ICP-MS

To determine lung burden of each metal after inhalation exposure, n = 5 female mice per each ENM, per each time point (4 and 24 h) were exposed to generated nanoparticulate aerosol, as described above. Control animals were exposed to HEPA-filtered laboratory air. The exposure concentrations in these dosimetry assessment studies are listed in Table 2. Left lobes of lung tissues (harvested from mice without BAL) were freeze dried (FreeZone,

Freeze Dry Systems, Labconco Co., Kansas City, MO) for 18 h and weighed using an analytical balance (Mettler Toledo, Mo. XPR206CDR). EPA Method 3051 was modified for digesting tissues from animals exposed to CuO, V_2O_5, and ZnO. Briefly, the entire left lobe (~8 mg) of lung tissue was weighed and transferred to a pre-weighed Teflon digestion vessel containing 9 mL of concentrated HNO_3 and 1 mL of 30% H_2O_2. Samples were then acid digested using a Milestone ETHOS UP (Sorisole, Italy) microwave digestion system with a ramp set to 210 °C for 20 min with a hold at 210 °C for 15 min. Samples were then diluted with 40 mL of deionized water. The digestion vessel mass was recorded again post digestion to obtain a final solution mass. Samples were then diluted 10-fold in 2% HNO_3 with 10 μg/L of ^{89}Y and ^{209}Bi as internal standards.

Studies have shown that tungsten chemistry, and solubility is complex, it can undergo polymerization in acidic conditions with HNO_3 and form precipitates, thus yielding measurements of aqueous which are a gross underestimation (Sun and Bostick, 2015; Bostick et al., 2018). To overcome this issue, a method by Griggs et al. (2009) was adapted for acid digestion of tissue samples from mice exposed to WO_3 carried out as described above but with 6 mL of HNO_3, 2 mL of H_3PO_4, and 10 mL of 30% H_2O_2. To determine the digestion efficiency, each ENMs (~0.5 mg) was digested using both EPA method 3051 and the Griggs et al. method. Percent recoveries were found to be 100%, 70%, 84%, and 92% for CuO, ZnO, V_2O_5, and WO_3, respectively. Further information on digestion efficiencies including a comparison between the two digestion methods is presented in supplementary materials (Supplementary Table 4). The concentrations of trace metals in lung tissue samples are expressed as μg/g of tissue (dry weight). All reagents were of trace metal grade or better. Digested samples were analyzed with inductively coupled plasma-mass spectrometry (ICP-MS, Agilent 7900, Santa Clara, CA) using helium gas in collision cell mode to remove isobaric interferences and increase sensitivity.

2.8. Statistical analyses

For the *in vitro* studies, the data were expressed as mean ± standard deviation. One-way analysis of variance (ANOVA) followed by Dunnett's *post hoc* test in GraphPad Prism (GraphPad Software, San Diego, CA) was used for statistical analysis of ENM characterization and cytotoxicity data. All outcome measures obtained from *in vivo* studies after exposure to ENMs were compared to sham-exposed animals using one-way ANOVA (Sigma Plot v.11.0, Systat Software Inc., Point Richmond, CA) followed by multiple comparison *versus* control group (Dunn's or Dunnett's Method). If data were not normally distributed, Kruskal-Wallis ANOVA on Ranks was used. A *t*-test was used to test differences in outcomes between males and females. A p-value < 0.05 was considered statistically significant. Statistical probability (p values) in plots is expressed as follows: ****$p < 0.0001$, ***$p < 0.001$, **$p < 0.01$, and *$p < 0.05$. Data are expressed as mean ± standard error (SE) unless otherwise noted.

3. Results and discussion

3.1. ENM characterization

Hydrodynamic diameter (dH) of ENM was determined using dynamic light scattering (DLS) technique. Mean intensity-weighted dH of ENM in SCM at 0 and 24 h was provided from NHIR ERCC as shown in Fig. 2a. Most ENMs exhibited consistent mean dH at 0 and 24 h suggesting these ENM formed agglomerates can be stably suspended in the presence of serum protein for at least 24 h except V_2O_5. The agglomerate sizes of WO_3, Al_2O_3, CeO_2, and Fe_2O_3 in SCM were generally 100–200 nm exhibiting a smaller degree of agglomeration than the other 5 ENMs, CuO, ZnO, V_2O_5, MgO, and TiO_2. These measured differences in aggregation may influence the delivered doses to cells for these materials, and therefore also affect the toxicity assessment.

ENMs dispersed in SFM were measured for dH only at 0 h as we observed that, after 24 h incubation of ENMs in SFM, aggregates formed that were visible to the naked eye and were very large and sedimented too rapidly to be measured using the Zetasizer. ENMs dispersed in SCM consistently displayed less agglomeration or aggregation than the SFM (Fig. 2a, c). This observation is consistent with the literature - others have reported less aggregation of nanomaterials in the presence of serum (Liu et al., 2015; Anders et al., 2015; Wells et al., 2012; Tedja et al., 2012). We confirmed that the use of serum containing media in *in vitro* assays is superior considering physiological conditions and such obtained results agree more closely with *in vivo* results. Serum proteins adsorbed onto nanoparticle surfaces form protein corona which is a key factor in nanoparticle-nanoparticle interactions and directly impact the cellular uptake of nanoparticles. Deguchi et al. demonstrated that NPs can adsorb serum protein to the surface and form a steric layer that can prevent the aggregation induced by salts present in cell culture media (Deguchi et al., 2007). The hydrodynamic size for all ENMs in SFM was usually > 1000 nm with the one exception being CuO ENMs (718.5 ± 58.2 nm) (Fig. 2c). The V_2O_5 and MgO showed high degree of aggregation immediately (t = 0 h) after preparation, therefore, the hydrodynamic size and particle size distribution of these ENMs could not be determined.

3.2. In vitro cytotoxicity using MTS assay

The cytotoxicity of ENMs to A549 cells was assessed using the colorimetric MTS assay for relative cell viability (Fig. 3). Materials that induced toxicity were defined as those that had significantly lower cell viability compared to the control group (cells that were incubated in either SFM or SCM and MTS reagent without any ENMs). The toxicity was assessed at 0.03, 5.0, 50, and 100 μg/mL of ENMs, which includes concentrations lower than what is typically reported in the literature (Pal et al., 2015; Wongrakpanich et al., 2016; Ahamed et al., 2010). For the present study it was imperative to investigate lower concentrations *in vitro* because the concentration of 0.03 μg/mL represents the epithelial surface-equivalent dose of the *in vivo* 4-h acute exposure at 3.5 mg/m^3 (Jing et al., 2015).

The results indicated that many of the metal oxide ENMs such as Al_2O_3, Fe_2O_3, CeO_2, TiO_2, MgO, and WO_3 did not demonstrate significant cytotoxicity at any concentration tested. However, CuO, ZnO, and V_2O_5 ENMs exhibited significant cytotoxicity at the

concentrations of 50 and 100 μg/mL at 4 and 24 h in SFM and SCM with the exception of the ZnO ENMs at 4 h in SCM (Fig. 3). Ahamed et al. reported that CuO ENMs reduced the relative cell viability of A549 cells after 24 h of exposure in a dose-dependent manner at 10–50 μg/mL (Ahamed et al., 2010). Wang et al. and Zhang et al. reported that ZnO ENMs decreased the relative viability of A549 cells after 24 h of exposure at 30 and 100 μg/mL (Zhang et al., 2017; Wang et al., 2018). It has also been reported that V_2O_5 ENMs induced cytotoxicity in A549 cells at much lower concentrations than observed in the current study, including 20, 30, and 40 μM (corresponding to 3.6, 5.5 and 7.3 μg/mL) (Karaboğa Arslan et al., 2017). Karlsson et al. investigated the cytotoxicity of different metal oxide NPs such as CuO, TiO_2, ZnO, $CuZnFe_2O_4$, Fe_3O_4 and Fe_2O_3 using A549 (Karlsson et al., 2008). Their results showed that CuO NPs had the highest cytotoxicity due to DNA damage, and they were the only NPs in the study that promoted a significant increase in intracellular reactive oxygen species (ROS). ZnO NPs were the second most toxic, as they induced DNA damage, however, not to the same extent as CuO NPs (Karlsson et al., 2008). A similar trend was observed in the present study, in that CuO and ZnO were the most toxic metal oxide ENMs investigated, but the toxicity of CuO ENMs were slightly higher than ZnO based on the 4-h incubation results shown in Fig. 3. Therefore, the DNA damage and formation of intracellular ROS may explain the toxicity of the CuO ENMs investigated herein.

The lowest concentrations of 0.03 and 5 μg/mL of each of the ENMs did not exhibit cytotoxicity in either SFM or SCM at 4- and 24-h incubation, with the exception of 5 μg/mL of 50 nm CuO ENMs in SFM after 24 h incubation (Fig. 3). In general, when ENMs were incubated with A549 cells in SCM they were less cytotoxic compared to the same dose of ENMs in SFM. In particular, the relative cell viability of CuO was only 15% after a 4 h incubation in SFM whereas it was 65% after 4 h in SCM at the highest dose of 100 μg/mL. A similar trend was observed for CuO ENMs after 24 h incubation in which the highest dose resulted in a viability of almost zero in SFM whereas it was approximately 7% in SCM. ZnO and V_2O_5 ENMs exhibited a similar trend. Saikia et al. found that the existence of protein corona on silica NPs in SCM mitigated the cytotoxicity compared to SFM conditions because of the decrease in cell-mediated uptake of the NPs (Saikia et al., 2016). The surface energy of NPs was reduced after the formation of a protein corona which inhibits NP adhesion to the cell surface decreasing particle internalization (Lesniak et al., 2012; Lesniak et al., 2013).

The Al_2O_3, Fe_2O_3 and TiO_2 ENMs induced increases in relative cell viability in a dose-dependent manner in SFM at 4 and 24 h (Fig. 3). This result might indicate an effect on cell proliferation of these materials, interference from ENM absorbance, or interactions between the dye and the ENMs. To address this concern, we tested the interference of ENMs with MTS reagent. The interference method is described in the Supplement. The result showed that only MgO 100 μg/mL caused a statistically significant increase in UV absorbance at 490 nm. In addition, V_2O_5 and CuO marginally, but not significantly, affected the readout/absorbance (Supplementary Fig. 1). In order to confirm the data obtained with MTS assay where cell viability (as opposed to interference) was measured, we performed an assay that did not rely on absorbance and instead directly assayed cell viability. Thus, viable cell counts were enumerated using propidium iodide (PI) staining (to stain dead cells) as an indicator of cytotoxicity as well as the effect of ENMs on cell proliferation.

3.3. In vitro cytotoxicity using viable cell count with PI staining

The viable cell count using PI staining was performed to assess cytotoxicity and cell proliferation effect to ensure no ENM interference. The toxicity for this test was assessed at 0.045, 7.5, 75, and 150 μg/mL ENMs in a 6-well plate with the same cell culture media condition and incubation time as the MTS assay. These concentrations are equivalent to those used in MTS assay base on ENM mass per surface area which are 0.009, 1.563, 15.625, and 31.25 $\mu g/cm^2$.

Materials that exhibited cytotoxicity were defined as those that had significantly lower viable cell count compared to the control group (cells that were incubated in either SFM or SCM without any ENMs). The result indicated that CuO, ZnO, and V_2O_5 exhibited the cytotoxicity in a dose dependent manner at 24 h in SFM and SCM and these 3 ENMs were more toxic than other 6 metal oxide ENMs (Fig. 4). This toxicity finding was similar to the result from MTS assay. However, the significant increases in % relative viable cell count compared to the control groups were found at a concentration of 7.5 μg/mL CuO at 4 h in SFM and the concentrations of 75 and 150 μg/mL MgO at 24 h in SFM. This indicated the cell proliferation effect on both ENMs occurred at specific concentration and only in SFM condition. CuO exhibited the cell proliferation effect only at a concentration of 7.5 μg/mL at 4 h in SFM can be explained as the copper was an essential element to promote cell growth and maintain healthy cells at the specific concentration. Typically, cell culture media does not contain elemental copper, but the copper was in sera that was used to supplement the media. The amount of copper sufficient for cell growth is 50 to 100 ng/mL which is contained in 5 to 10% sera (Millipore Sigma, 2020). This explanation supports that adding specific amount of CuO to the cells in SFM could increase cell proliferation. D'Mello et al. showed that inclusion of copper in chitosan based scaffolds enhanced bone tissue regeneration (D'Mello et al., 2015). MgO in SFM had greater opportunity to react with water molecule and form magnesium hydroxide ($MgO + H_2O \rightarrow Mg(OH)_2$) than in SCM since there is no serum protein binding at the surface of MgO to reduce the reaction between MgO and water (ERCC). Mg^{2+} can be dissociated from $Mg(OH)_2$ and stimulate cell proliferation as Mg promoted DNA and protein synthesis (Xing et al., 2018; Wolf and Cittadini, 1999).

There were no significant increases in % relative viable cell count on Al_2O_3, Fe_2O_3, and TiO_2 in SFM at 4 and 24 h as we found from MTS assay result. Therefore, we can conclude that these 3 ENMs had no proliferation effect and the finding from MTS assay could result from the artifactual interference from ENM absorbance.

3.4. Delivered-to-cell dose of ENMs

Nanomaterial dosimetry provides meaningful and important information for *in vitro* cytotoxicity screening as the dose delivered to cells represents a more accurate measure of ENM dose than the nominal administered dose (DeLoid et al., 2015). The reason is because ENMs generally form agglomerates when dispersed in any liquid and these agglomerates have a specific sedimentation rate as a function of exposure time. The particle size distribution and effective density of these agglomerates affects the sedimentation rate of ENMs as shown in Eq. (1)

$$V_s = \frac{g(\rho_{EV} - \rho_{media})d_H^2}{18\eta} \quad (1)$$

where g is acceleration due to gravity (m s^{-2}), ρ_{EV} is effective density of particle (kg m^{-3}), ρ_{media} is media density (kg m^{-3}), and η is the media dynamic viscosity (kg m^{-1} s^{-1}). Thus, the sedimentation velocity is proportional to the difference between the effective densities of particle and the densities of suspending media and the square of the suspended particle diameter (DeLoid et al., 2017a; DeLoid et al., 2015). Based on this equation, the agglomeration size influences sedimentation rate and therefore the dose delivered to the cell surface.

The mean volume-weighted dH, effective density, and delivered-to-cell doses of ENM in SCM were provided from NHIR ERCC as shown in Table 1 (we did not validate these data). The delivered-to-cell doses data would allow dosimetry-based toxicity assessment as described by DeLoid et al. (2017a, 2017b). The order from largest to smallest agglomeration size exhibited as follows: MgO, ZnO, TiO_2, V_2O_5, CuO, Fe_2O_3, CeO_2, Al_2O_3, and WO_3. The first 4 largest ENMs also showed the highest mass of ENM delivered to cells. Similarly, the smallest agglomerate, WO_3 had the smallest mass ENMs delivered to the cells. This finding was reasonable according to the previous explanation from Eq. (1).

The mass of ENM delivered to the cells in SFM is expected to be greater than in SCM since the agglomerate size for most ENMs in SFM was greater than in SCM. This explains our viable cell count cytotoxicity data for CuO and ZnO at 4 h incubation showing that ENMs in SFM exhibited more toxicity than in SCM.

The % relative viable cell count for CuO, ZnO, and V_2O_5 at 24 h incubation in SCM was plotted against the dosimetry dose based concentration (Supplementary Fig. 2) that was calculated by multiplying the mean fraction of deposited ENMs for 24 h and the nominal concentration. This figure showed that CuO induced the highest cytotoxicity.

3.5. Characterization of generated ENM aerosol for in vivo exposures

The conditions for the generation of nanoaerosol and exposure of mice in our nose-only system were meticulously controlled. The mass concentration of aerosol was held to our target of 3.5 mg/m^3 by controlling the pressure, flow rate and mass of suspended nanomaterial in the Collison nebulizer. The exposure concentration was selected based on our (Adamcakova-Dodd et al., 2014; Adamcakova-Dodd et al., 2015; Kim et al., 2011) and other's (Gosens et al., 2016) previous studies investigating various ENMs, as well as considering relevance to potential human exposures. The exact mass of each ENMs used in the nebulizer for the aerosol generation is reported in Table 2. Higher masses of nanomaterials were used for V_2O_5 and CuO aerosol generation (1 mg/mL), followed by ZnO and WO_3 (0.3 and 0.4 mg/mL, respectively). We were able to achieve very similar exposure concentrations for all materials (Table 2), all were in the range between 3.24 and 4.15 mg/m^3. The smallest geometric mean mobility diameter (GM) of generated particles was measured for CuO (33.26 nm), followed by ZnO (37.54 nm) and V_2O_5 (43.03 nm). The largest GM was generated for WO_3 aerosol (77.61 nm) as shown in Table 2. Comparing the

GM of the aerosol size distribution with the primary ENM particle sizes reported in Supplementary Table 1, the smallest primary sized particles, WO_3 (20 nm) generated the highest agglomeration/aggregation of particles. Peak particle counts were all similar with the highest counts for V_2O_5 (Table 2, Fig. 5). We also measured the particle size distribution of particulates/contaminants that are always present in water (Fig. 5). The particle size distribution of all ENMs reported in Fig. 5 contains a small fraction of particles derived from the water (Knight and Petrucci, 2003). Since pure, analytical grade water was used as a vehicle for the generation of ENM aerosol the contribution of contaminant particle counts to the total measured was relatively insignificant.

3.6. In vivo pulmonary responses after acute exposures

The inflammatory potency of ENMs after 4 h exposure was assessed by the evaluation of cells obtained by BAL, cell viability, total protein, cytokine concentrations and histopathology evaluation of lung tissues. There was a significantly higher recruitment of cells into the lungs in ZnO-exposed male mice at the 4 h time point (Fig. 6) in comparison to shams. At the 24 h time point, the total number of cells increased in both males and females in CuO- and ZnO-exposed mice compared to shams, however this increase was shown to be significant only in males due to a higher variability in females. There was a significant increase in the number of total cells in male ZnO-exposed mice at 4 h time point compared to female counterparts, however there was no significant difference between males and females at 24 h. The number of neutrophils in BAL fluid was slightly increased in CuO- and ZnO-exposed mice, both males and females at the 4-h time point (Fig. 7); however this increase was statistically significant only for CuO-exposed females. We observed much higher neutrophilic recruitment at the 24-h time point for the same ENMs in both, males and females. The number of lymphocytes was also significantly increased compared to shams in ZnO-exposed mice in both, male and females. The proportion of neutrophils in BAL fluid in CuO-exposed mice was increased from about 2% at 4 h to 56 ± 4% in females and to 61 ± 9% in males at 24 h (Fig. 8). In ZnO-exposed mice, this increase was from about 2 ± 0.5% at 4 h to 42 ± 8% at 24 h in females and from 1 ± 0.2% to 27 ± 6% in males. The number of eosinophils found in BAL fluid was not significantly increased at any time point after exposure, sex or type of ENM.

The viability of total cells that included the cells with the wider size range (6.5–23 μm) was decreased compared with sham-exposed mice after ZnO and CuO exposure at the 24 h time point in both, females and males (Fig. 9A and B). When we analyzed the viability of the cells with the cell diameter in the size range of mouse monocytes/macrophages (9.5 and 21.5 μm), we found a larger decrease in the viability compared to controls in ZnO and CuO-exposed mice at 24 h (Fig. 9C and D). The results of total protein determination support higher cell injury for ZnO-exposed animals at 24 h compared to shams or CuO-exposed mice (Supplementary Fig. 3).

The concentrations of selected inflammatory cytokines/chemokines confirm the inflammatory responses after exposure to ZnO and CuO ENMs. However significant differences between CuO and ZnO ENMs in lavage cytokines were observed, indicating involvement different immunotoxicity pathways in inflammatory responses between these

two ENMs (Fig. 10). The release of IL-6 in the lungs, the major mediator of the acute phase inflammation (Tanaka et al., 2014), was significantly higher in both females and males (1227 and 966 pg/mL, respectively) at the 4 h time point after ZnO exposure compared to controls or CuO ENM exposure (< 2.26 pg/mL [LLOD]). This increase was not observed after CuO exposure. At the 24 h time point after ZnO exposure, IL-6 concentrations decreased significantly in both females and males (146 and 126 pg/mL, respectively). Such a release of IL-6 is indicative of inflammation associated with lung tissue injury and increased total protein release at 24 h post exposure, as observed after ZnO exposure. Early release of IL-6 into circulation or BAL fluid was observed in workers after single exposure to ZnO fume after 2 h-exposure to 5 mg/m^3 (Fine et al., 1997; Fine et al., 2000). Workers in that study, were exposed to freshly generated ZnO vapor condensed to ultrafine particles with the mass median diameter of 0.3 μm. Upregulation of IL-6 was also observed after acute (3-day) ZnO NP exposure of female ICR mice by inhalation (Rossner Jr et al., 2018). Acute exposure to CuO ENM caused higher release of keratinocyte-derived chemokine (KC) (neutrophil chemoattractant released by macrophages, neutrophils and epithelial cells) especially at 24 h post exposure in comparison to controls or ZnO exposure, even though both, CuO and ZnO caused a high number of neutrophils in BAL fluid. In agreement with the neutrophilic recruitment into BAL fluid 24 h post exposure, the concentration of KC was higher after CuO exposure than after ZnO exposure at the 24 h time point.

Most of the evaluated tissues had nominal or focal changes that were often in the lowest thresholds of detection. Supplementary Table 2 reports on the scores of the changes evaluated. A 5-point scale was used for the evaluation of potential pathologies. All of the tissues were scored either with the score of 0 (within the scope of normal), 1 (rare, but detectable change), or 2 (mild in distribution/severity). Increased numbers of macrophages and activated macrophages were found after CuO exposures in both females (average score of 1.8 ± 0.1) and males (1.2 ± 0.1). The most noticeable changes were represented by the presence of neutrophils around vessels (perivascular infiltration or aggregates) found for V_2O_5, in both time points post exposure and in females and males, however these changes were still scored as mild. None of the tissues were scored with moderate (score 3) or severe (score 4) in distribution/severity in any evaluated changes. Consistent with the results from BAL fluid, observed changes were more pronounced at the 24-h time point compared to the 4-h time point in all materials showing some inflammatory responses (CuO and ZnO). Supplementary Fig. 4 shows representative micrographs of lung tissues after V_2O_5 exposure (with a histology score 2 for perivascular infiltration of leukocytes around vessels at each time point for each sex), pointing out that all observed changes were minimal.

The effects of various types of ENMs after inhalation exposure differ by the duration and severity of the responses. The results of our studies confirmed the toxicity of CuO (Pettibone et al., 2008; Kim et al., 2011) and ZnO ENMs after inhalation exposure seen in many other inhalation studies (Chuang et al., 2014; Vandebriel and De Jong, 2012; Larsen et al., 2016), however the number of studies using only an acute protocol with shorter-term exposure for screening ENMs is limited (Gosens et al., 2016; Larsen et al., 2016). In our studies we also found that at least two time points post-acute exposure (*e.g.* 4 and 24 h) should be investigated to explore the toxicity of ENMs. Even though our *in vitro* screening assay did not point to an increased cytotoxicity of WO_3, due to the lack of toxicological data after

respiratory exposure, we thought to include this material in our *in vivo* acute screening protocol and compare the toxicity with other studied ENMs. None of the results of our WO_3 inhalation study showed significant differences compared to controls. The recruitment of neutrophils into the lungs (Fig. 8) after WO_3 exposure was < 2% in all experimental groups (ranging from 0.8% to 1.6%) and similar to sham-exposed mice (0.3% - 0.7%). In an inhalation study of WO_3 NPs in golden Syrian hamsters (Prajapati et al., 2017), animals were exposed in a whole-body exposure chamber to low or high concentration (5 or 10 mg/m^3, respectively) for 4 h/day for 4 or 8 days. An average geometric mean particle diameter of WO_3 particulates produced in this study was 202 ± 49 nm. After inhalation exposure of WO_3 particulate aerosol for 4 days, pulmonary inflammation (represented by an increase of neutrophils in BAL fluid) was significantly increased with the higher exposure concentration (10 mg/m^3), but not with lower exposure concentration (5 mg/m^3). In our studies, we did not see significant pulmonary inflammation or immunotoxicity after V_2O_5 ENM exposure, as has been described elsewhere (Worle-Knirsch et al., 2007; Kulkarni et al., 2014). Also, our *in vitro* screening studies showed that these materials lowered the relative cell viability. However most of the studies of V_2O_5 NPs were conducted *in vitro* or *in vivo* with repeated exposures (Kulkarni et al., 2014; Karaboğa Arslan et al., 2017). The toxicity of bulk vanadium pentoxide after inhalation exposures has been studied (Dill et al., 2004; Cooper, 2007; NTP toxicology and carcinogensis studies of vanadium pentoxide (CAS No. 1314–62-1) in F344/N rats and B6C3F1 mice (inhalation), 2002). The differences observed between *in vitro* and *in vivo* results in our screening studies might be due to short half-life of V_2O_5 after inhalation (Conklin et al., 1982). One hour after intratracheal instillation of 0.5 μCi ^{48}V in V_2O_5 form (0.3 mg/kg, 40 μg/rat), 40% of the total ^{48}V had been cleared, by day 3, 90% had been cleared (Conklin et al., 1982). Faster elimination of V_2O_5 has been reported in mice than rats (Dill et al., 2004). Such rapid clearance of V_2O_5 after acute exposure (which was not verified for nanoparticulate form of V_2O_5) might be responsible for the lack of toxicity present after acute inhalation exposure. The absence of clearance mechanisms in *in vitro* studies especially at submersed conditions (which is one of the limitations of such studies) must always be considered when comparing *in vitro* and *in vivo* screening methods. In our *in vivo* studies, retained doses of each particular ENM were determined using ICP-MS as reported in Table 4. We found higher clearance of W and V from the lungs than Cu at the 24 h time point post exposure. The lung burden of W decreased 3-fold in 24 h (from 58.6 μg/g at 4 h to 19.8 μg/g at 24 h). More than half of the V was cleared from the lungs 24 h post exposure (32 μg/g at 4 h and 18 μg/g at 24 h). Our estimations of deposited doses in the lungs using MPPD modeling (Table 3) agreed closely with our values measured by ICP-MS (Table 4) for all materials except ZnO. Concentration of Zn in the lungs after 4 h exposure was not significantly different from sham-exposed animals. We have seen similar results in our previous studies after sub-acute or sub-chronic inhalation exposure to ZnO nanomaterials (Adamcakova-Dodd et al., 2014).

We hypothesize that rapid dissolution of ZnO NPs in lung fluids is a possible mechanism for the clearance of ENMs. To test this, we compared experimental data (observed) to theoretical dissolution data (modeled) for selected materials. Dissolution of ENMs was modeled using Visual MINTEQ (Gustafsson, 2011). Dissolution modeling was done for selected ENMs such as CuO (tenorite), ZnO (zincite) and V_2O_5 from our *in vivo* studies.

Literature on tungsten is limited and ionic equilibrium data for WO_3 was not available - this prevented us from modeling its dissolution. We simulated two physiologically relevant chemical conditions which include artificial lysosomal fluid (ALF, pH 4.5) and Gamble's solution (pH 7.4). Components used to build these two simulations were those used for the measured dissolution experiments (Stopford et al., 2003; Midander et al., 2007; Moss, 1979). Results from our model (Supplemental Table 5) suggest that in ALF, we expect to see 100% of the CuO and ZnO dissolved while there will be very little dissolution of V_2O_5. This finding might serve to explain the loss of macrophage viability at both 4 h and 24 h for ZnO and CuO not seen for V_2O_5 resulting from rapid increase in metal ion concentration in the lysosome from rapid dissolution of the metal oxides. Interestingly, the opposite trend is observed for Gamble's solution where we expect to see 100% dissolution of V_2O_5 but very little for CuO and ZnO.

Results from our dissolution modeling is supported by dissolution experiment results previously published by our group which also showed 100% of ZnO dissolved within 24 h in ALF, but < 1% in Gamble's solution after 2 wks (Adamcakova-Dodd et al., 2014). Similarly, in our previous studies, CuO ENMs dissolved more in ALF than in Gamble's solution (pH 7.4) (Pettibone et al., 2008). Based on our previous studies (Adamcakova-Dodd et al., 2014; Pettibone et al., 2008), the dissolution rates of ZnO and CuO were similar, however we observed lower clearance for Cu (Supplemental Table 5). V_2O_5 (fine powder, geometric mean diameter 0.31 μm) was found to be 8 times more soluble in Gamble's solution than in a pure water (Toya et al., 2001). Based on our results from *in vitro* screening as well as considering known toxicity of bulk V_2O_5, a subacute or chronic inhalation exposure study is warranted to further assess the toxicity of this ENM. Determination of the dissolution characteristics of all studied materials in various simulated physiological conditions is a critical step towards explaining their higher or lower clearance and subsequent toxicity. This novel modeling approach might be a rapid, cost effective *in silico* tool for screening large quantities of ENMs in multiple simulated physiochemical conditions in addition to the lung, such as gastric fluid having pH < 2 would certainly change the dissolution kinetics of ENMs. This tool and possibly in conjunction with machine learning techniques also opens up the possibility of looking at dissolution of mixtures of ENMs leading to more environmentally relevant toxicity assessments. Further experimental studies are warranted to confirm and improve this newly emerging modeling approach.

A slight increase in the recruitment of total cells into the lungs at the 4 h time point was observed in males compared to females after exposure to ZnO ENMs (Fig. 6, $p < 0.001$). Conversely the concentration of IL-6 in BAL fluid also at the 4 h time point was higher in females (1227 ± 188 pg/mL) than males (966 ± 102 pg/mL), but not significantly (Fig. 10), and concentration of G-CSF in BAL fluid at 24 h time point was significantly higher (Fig. 10, $p < 0.01$) in females (319 ± 37 pg/mL) than males (138 ± 16 pg/mL). None of the other materials studied showed sex differences.

4. Conclusion

We aimed to establish a toxicity screening method for inhaled ENMs using *in vitro* and *in vivo* acute protocols. The *in vitro* assessments were conducted with the intention of a rapid

screening of ENMs for their potential toxicities while the *in vivo* assessment was conducted to confirm or rebut the *in vitro* results in a model more relevant to human exposure. The results of a viability assay performed after exposure of A549 cells at submersed conditions were in the agreement with our *in vivo* results after acute nose-only inhalation exposure of C57Bl/6 mice for CuO, ZnO, and WO_3 ENMs. However, the V_2O_5 ENMs showed a dose-dependent toxicity *in vitro* that was not observed *in vivo*. From all studied ENMs: ZnO, CuO, CeO_2, Fe_2O_3, WO_3, V_2O_5, TiO_2, Al_2O_3 and MgO, the highest toxicity was shown for CuO and ZnO ENMs. The assessment of cell viability after *in vitro* exposure and lung inflammation after acute inhalation exposure *in vivo* were shown to be sensitive endpoints to predict toxicity after a short-term exposure. Two time points (4 and 24 h) after acute (one-time) inhalation exposure were necessary to observe inflammation from studied ENMs.

Supplementary Material

Refer to Web version on PubMed Central for supplementary material.

Acknowledgements

Research reported in this publication was supported by the National Institute of Environmental Health Sciences of the National Institutes of Health under Award Number [NIH grant # U01ES027252] as part of the Nanotechnology Health Implications Research (NHIR) Consortium which focuses on comprehensive evaluation of interactions between ENMs and biological systems. The research was conducted in laboratory facilities supported by the Environmental Health Sciences Research Center funded by NIH P30 ES005605. The content is solely the responsibility of the authors and does not necessarily represent the official views of the National Institutes of Health.

The engineered nanomaterials used in the research presented in this publication have been procured/developed, characterized, and provided by the Engineered Nanomaterials Resource and Coordination Core established at Harvard T. H. Chan School of Public Health (NIH grant # U24ES026946) as part of the NHIR Consortium.

The research was conducted in laboratory facilities supported by the Environmental Health Sciences Research Center funded by NIH P30 ES005605. B.E.G. was supported by the Alfred P. Sloan Foundation Minority PhD Scholarship, National GEM Consortium Associate Fellowship, The University of Iowa Graduate College Dean's Fellowship. A.K.S. was supported by the Lyle & Sharon Bighley Endowed Professorship. We thank Dr. Xuefang Jing for her help with necropsies.

References

Adamcakova-Dodd A, Stebounova LV, Kim JS, Vorrink SU, Ault AP, O'Shaughnessy PT, Grassian VH, Thorne PS, 2014 Toxicity assessment of zinc oxide nanoparticles using sub-acute and sub-chronic murine inhalation models. Particle and Fibre Toxicology. 11 (1), 15 10.1186/1743-8977-11-15. [PubMed: 24684892]

Adamcakova-Dodd A, Monick MM, Powers LS, Gibson-Corley KN, Thorne PS, 2015 Effects of prenatal inhalation exposure to copper nanoparticles on murine dams and offspring. Particle and Fibre Toxicology. 12 (1), 30 10.1186/s12989-015-0105-5. [PubMed: 26437892]

Ahamed M, Siddiqui MA, Akhtar MJ, Ahmad I, Pant AB, Alhadlaq HA, 2010 Genotoxic potential of copper oxide nanoparticles in human lung epithelial cells. Biochem. Biophys. Res. Commun. 396 (2), 578–583. 10.1016/j.bbrc.2010.04.156 (Epub 2010/05/08, PubMed PMID: 20447378). [PubMed: 20447378]

Ahamed M, Akhtar MJ, Alhadlaq HA, Alrokayan SA, 2015 Assessment of the lung toxicity of copper oxide nanoparticles: current status. Nanomedicine 10, 2365+. [PubMed: 26251192]

Anders CB, Chess JJ, Wingett DG, Punnoose A, 2015 Serum proteins enhance dispersion stability and influence the cytotoxicity and dosimetry of ZnO nanoparticles in suspension and adherent cancer cell models. Nanoscale Res. Lett. 10 (1), 448 10.1186/s11671-015-1158-y. [PubMed: 26577392]

Andreescu S, Ornatska M, Erlichman JS, Estevez A, Leiter JC, 2012 Biomedical applications of metal oxide nanoparticles In: Matijević E (Ed.), Fine Particles in Medicine and Pharmacy. Springer US, Boston, MA, pp. 57–100.

Asgharian B, Price OT, Oldham M, Chen LC, Saunders EL, Gordon T, Mikheev VB, Minard KR, Teeguarden JG, 2014 Computational modeling of nanoscale and microscale particle deposition, retention and dosimetry in the mouse respiratory tract. Inhalation toxicology 26 (14), 829–842. 10.3109/08958378.2014.935535 (Epub 2014/11/07, PubMed PMID: 25373829; PMCID: PMC4668803). [PubMed: 25373829]

Bakand S, Winder C, Khalil C, Hayes A, 2005 Toxicity assessment of industrial chemicals and airborne contaminants: transition from in vivo to in vitro test methods: a review. Inhal. Toxicol. 17 (13), 775–787. 10.1080/08958370500225240 (Epub 2005/10/01, PubMed PMID: 16195213). [PubMed: 16195213]

Beltran-Huarac J, Zhang Z, Pyrgiotakis G, DeLoid G, Vaze N, Demokritou P, 2018 Development of reference metal and metal oxide engineered nanomaterials for nanotoxicology research using high throughput and precision flame spray synthesis approaches. NanoImpact. 10, 26–37. 10.1016/j.impact.2017.11.007. [PubMed: 30035243]

Bostick BC, Sun J, Landis JD, Clausen JL, 2018 Tungsten speciation and solubility in munitions-impacted soils. Environmental science & technology. 52 (3), 1045–1053. 10.1021/acs.est.7b05406. [PubMed: 29307178]

Chavali MS, Nikolova MP, 2019 Metal oxide nanoparticles and their applications in nanotechnology. SN Applied Sciences. 1 (6), 607 10.1007/s42452-019-0592-3.

Chuang HC, Juan HT, Chang CN, Yan YH, Yuan TH, Wang JS, Chen HC, Hwang YH, Lee CH, Cheng TJ, 2014 Cardiopulmonary toxicity of pulmonary exposure to occupationally relevant zinc oxide nanoparticles. Nanotoxicology. 8 (6), 593–604. 10.3109/17435390.2013.809809 (Epub 2013/06/07, PubMed PMID: 23738974). [PubMed: 23738974]

Cohen JM, Beltran-Huarac J, Pyrgiotakis G, Demokritou P, 2018 Effective delivery of sonication energy to fast settling and agglomerating nanomaterial suspensions for cellular studies: implications for stability, particle kinetics, dosimetry and toxicity. NanoImpact. 10, 81–86. 10.1016/j.impact.2017.12.002. [PubMed: 29479575]

Conklin AW, Skinner CS, Felten TL, Sanders CL, 1982 Clearance and distribution of intratracheally instilled 48Vanadium compounds in the rat. Toxicology letters 11 (1), 199–203. 10.1016/0378-4274(82)90128-X. [PubMed: 7090012]

Cooper RG, 2007 Vanadium pentoxide inhalation. Indian J Occup Environ Med. 11 (3), 97–102. 10.4103/0019-5278.38457 (PubMed PMID: 21957373). [PubMed: 21957373]

Deguchi S, Yamazaki T, Mukai S, Usami R, Horikoshi K, 2007 Stabilization of C60 nanoparticles by protein adsorption and its implications for toxicity studies. Chem. Res. Toxicol. 20 (6), 854–858. 10.1021/tx6003198. [PubMed: 17503852]

DeLoid GM, Cohen JM, Pyrgiotakis G, Pirela SV, Pal A, Liu J, Srebric J, Demokritou P, 2015 Advanced computational modeling for in vitro nanomaterial dosimetry. Particle and Fibre Toxicology. 12 (1), 32 10.1186/s12989-015-0109-1. [PubMed: 26497802]

DeLoid GM, Cohen JM, Pyrgiotakis G, Demokritou P, 2017a Preparation, characterization, and in vitro dosimetry of dispersed, engineered nanomaterials. Nature protocols 12 (2), 355–371. 10.1038/nprot.2016.172 (Epub 2017/01/20, PubMed PMID: 28102836; PMCID: PMC5857388). [PubMed: 28102836]

DeLoid GM, Wang Y, Kapronezai K, Lorente LR, Zhang R, Pyrgiotakis G, Konduru NV, Ericsson M, White JC, De La Torre-Roche R, Xiao H, McClements DJ, Demokritou P, 2017b An integrated methodology for assessing the impact of food matrix and gastrointestinal effects on the biokinetics and cellular toxicity of ingested engineered nanomaterials. Particle and Fibre Toxicology. 14 (1), 40 10.1186/s12989-017-0221-5. [PubMed: 29029643]

Dill JA, Lee KM, Mellinger KH, Bates DJ, Burka LT, Roycroft JH, 2004 Lung deposition and clearance of inhaled vanadium pentoxide in chronically exposed F344 rats and B6C3F1 mice. Toxicological sciences: an official journal of the Society of Toxicology. 77 (1), 6–18. 10.1093/toxsci/kfh005 (Epub 2003/11/06, PubMed PMID: 14600283). [PubMed: 14600283]

D'Mello S, Elangovan S, Hong L, Ross RD, Sumner DR, Salem AK, 2015 Incorporation of copper into chitosan scaffolds promotes bone regeneration in rat calvarial defects. Journal of biomedical

materials research Part B, Applied biomaterials 103 (5), 1044–1049. 10.1002/jbm.b.33290 (Epub 2014/09/18, PubMed PMID: 25230382; PMCID: PMC4363304).

Fine JM, Gordon T, Chen LC, Kinney P, Falcone G, Beckett WS, 1997 Metal fume fever: characterization of clinical and plasma IL-6 responses in controlled human exposures to zinc oxide fume at and below the threshold limit value. J. Occup. Environ. Med. 39 (8), 722–726 (Epub 1997/08/01, PubMed PMID: 9273875). [PubMed: 9273875]

Fine JM, Gordon T, Chen LC, Kinney P, Falcone G, Sparer J, Beckett WS, 2000 Characterization of clinical tolerance to inhaled zinc oxide in naive subjects and sheet metal workers. J. Occup. Environ. Med. 42 (11), 1085–1091. 10.1097/00043764-200011000-00010 (PubMed PMID: 11094787). [PubMed: 11094787]

Golbamaki N, Rasulev B, Cassano A, Marchese Robinson RL, Benfenati E, Leszczynski J, Cronin MTD, 2015 Genotoxicity of metal oxide nanomaterials: review of recent data and discussion of possible mechanisms. Nanoscale. 7 (6), 2154–2198. 10.1039/C4NR06670G. [PubMed: 25580680]

Gosens I, Cassee FR, Zanella M, Manodori L, Brunelli A, Costa AL, Bokkers BGH, de Jong WH, Brown D, Hristozov D, Stone V, 2016 Organ burden and pulmonary toxicity of nano-sized copper (II) oxide particles after short-term inhalation exposure. Nanotoxicology. 10 (8), 1084–1095. 10.3109/17435390.2016.1172678 (Epub 2016/05/02, PubMed PMID: 27132941). [PubMed: 27132941]

Grassian VH, O'Shaughnessy PT, Adamcakova-Dodd A, Pettibone JM, Thorne PS, 2007 Inhalation exposure study of titanium dioxide nanoparticles with a primary particle size of 2 to 5 nm. Environmental health perspectives 115 (3), 397–402. 10.1289/ehp.9469 (Epub 2007/04/14, PubMed PMID: 17431489; PMCID: PMC1849915). [PubMed: 17431489]

Griggs CS, Larson S, Nestler C, Wynter M, 2009 Coupling of oxygen and pH requirements for effective microwave-assisted digestion of soils for tungsten analysis. Land Contamination & Reclamation. 17, 121–128. 10.2462/09670513.927.

Gröhn AJ, Pratsinis SE, Sánchez-Ferrer A, Mezzenga R, Wegner K, 2014 Scale-up of nanoparticle synthesis by flame spray pyrolysis: the high-temperature particle residence time. Ind. Eng. Chem. Res. 53 (26), 10734–10742. 10.1021/ie501709s.

Gustafsson JP, 2011 Visual MINTEQ 3.0 User Guide. KTH, Department of Land and Water Recources, Stockholm, Sweden.

Holder AL, Goth-Goldstein R, Lucas D, Koshland CP, 2012 Particle-induced artifacts in the MTT and LDH viability assays. Chem Res Toxicol. 25 (9), 1885–1892. 10.1021/tx3001708 (Epub 2012/07/18, PubMed PMID: 22799765; PMCID: PMC3446248). [PubMed: 22799765]

Jing X, Park JH, Peters TM, Thorne PS, 2015 Toxicity of copper oxide nanoparticles in lung epithelial cells exposed at the air–liquid interface compared with in vivo assessment. Toxicol. in Vitro 29 (3), 502–511. 10.1016/j.tiv.2014.12.023. [PubMed: 25575782]

Karaboğa Arslan A, Öztürk E, Yerer M, 2017 Monitoring the Effectiveness and Time Dependency of Vanadium Pentoxide Cytotoxicity on A549 and Beas-2b Cell Lines. pp. 5.

Karlsson HL, Cronholm P, Gustafsson J, Möller L, 2008 Copper oxide nanoparticles are highly toxic: a comparison between metal oxide nanoparticles and carbon nanotubes. Chem. Res. Toxicol. 21 (9), 1726–1732. 10.1021/tx800064j. [PubMed: 18710264]

Kim JS, Adamcakova-Dodd A, O'Shaughnessy PT, Grassian VH, Thorne PS, 2011 Effects of copper nanoparticle exposure on host defense in a murine pulmonary infection model. Part Fibre Toxicol. 8, 29 10.1186/1743-8977-8-29 (Epub 2011/09/29, PubMed PMID: 21943386; PMCID: PMC3193802). [PubMed: 21943386]

Knight M, Petrucci GA, 2003 Study of residual particle concentrations generated by the ultrasonic nebulization of deionized water stored in different container types. Anal. Chem. 75 (17), 4486–4492. 10.1021/ac034355n. [PubMed: 14632054]

Kulkarni A, Kumar GS, Kaur J, Tikoo K, 2014 A comparative study of the toxicological aspects of vanadium pentoxide and vanadium oxide nanoparticles. Inhal. Toxicol. 26 (13), 772–788. 10.3109/08958378.2014.960106 (Epub 2014/10/10, PubMed PMID: 25296879). [PubMed: 25296879]

Lai X, Zhao H, Zhang Y, Guo K, Xu Y, Chen S, Zhang J, 2018 Intranasal delivery of copper oxide nanoparticles induces pulmonary toxicity and fibrosis in C57BL/6 mice. Sci. Rep. 8 (1), 4499 10.1038/s41598-018-22556-7. [PubMed: 29540716]

Larsen ST, Jackson P, Poulsen SS, Levin M, Jensen KA, Wallin H, Nielsen GD, Koponen IK, 2016 Airway irritation, inflammation, and toxicity in mice following inhalation of metal oxide nanoparticles. Nanotoxicology. 10 (9), 1254–1262. 10.1080/17435390.2016.1202350 (Epub 2016/07/18, PubMed PMID: 27323801). [PubMed: 27323801]

Lee JY, Wang H, Pyrgiotakis G, DeLoid GM, Zhang Z, Beltran-Huarac J, Demokritou P, Zhong W, 2018 Analysis of lipid adsorption on nanoparticles by nanoflow liquid chromatography-tandem mass spectrometry. Anal. Bioanal. Chem. 410 (24), 6155–6164. 10.1007/s00216-018-1145-0. [PubMed: 29845324]

Lesniak A, Fenaroli F, Monopoli MP, Aberg C, Dawson KA, Salvati A, 2012 Effects of the presence or absence of a protein corona on silica nanoparticle uptake and impact on cells. ACS Nano 6 (7), 5845–5857. 10.1021/nn300223w (Epub 2012/06/23, PubMed PMID: 22721453). [PubMed: 22721453]

Lesniak A, Salvati A, Santos-Martinez MJ, Radomski MW, Dawson KA, Aberg C, 2013 Nanoparticle adhesion to the cell membrane and its effect on nanoparticle uptake efficiency. J. Am. Chem. Soc. 135 (4), 1438–1444. 10.1021/ja309812z (Epub 2013/01/11, PubMed PMID: 23301582). [PubMed: 23301582]

Liu R, Liu HH, Ji Z, Chang CH, Xia T, Nel AE, Cohen Y, 2015 Evaluation of toxicity ranking for metal oxide nanoparticles via an in vitro dosimetry model. ACS Nano 9 (9), 9303–9313. 10.1021/acsnano.5b04420. [PubMed: 26284985]

Louro H, Saruga A, Santos J, Pinhao M, Silva MJ, 2019 Biological impact of metal nanomaterials in relation to their physicochemical characteristics. Toxicology in vitro: an international journal published in association with BIBRA. 56, 172–183. 10.1016/j.tiv.2019.01.018 (Epub 2019/02/02, PubMed PMID: 30707927). [PubMed: 30707927]

Meyerholz DK, Beck AP, 2018 Principles and approaches for reproducible scoring of tissue stains in research. Lab. Investig. 98 (7), 844–855. 10.1038/s41374-018-0057-0. [PubMed: 29849125]

Meyerholz DK, Sieren JC, Beck AP, Flaherty HA, 2018 Approaches to evaluate lung inflammation in translational research. Veterinary pathology 55 (1), 42–52. 10.1177/0300985817726117 (Epub 2017/08/16, PubMed PMID: 28812529; PMCID: PMC5600706). [PubMed: 28812529]

Midander K, Pan J, Wallinder IO, Heim K, Leygraf C, 2007 Nickel release from nickel particles in artificial sweat. Contact Dermatitis 56 (6), 325–330. 10.1111/j.1600-0536.2007.01115.x. [PubMed: 17577373]

Millipore Sigma, Jan 21, 2020. Copper in cell culture 2020 Available from: https://www.sigmaaldrich.com/life-science/cell-culture/learning-center/media-expert/copper.html.

Moss OR, 1979 Simulants of lung interstitial fluid. Health Phys. 36 (3), 447–448 (PubMed PMID: 489300). [PubMed: 489300]

Navrotsky A, 2001 Thermochemistry of nanomaterials. Rev. Mineral. Geochem. 44 (1), 73–103. 10.2138/rmg.2001.44.03.

NTP toxicology and carcinogensis studies of vanadium pentoxide (CAS No. 1314–62-1) in F344/N rats and B6C3F1 mice (inhalation). In: National Toxicology Program Technical Report Series 507. pp. 1–343 (Epub 2003/01/21. PubMed PMID: 12533744).

Pal AK, Bello D, Cohen J, Demokritou P, 2015 Implications of in vitro dosimetry on toxicological ranking of low aspect ratio engineered nanomaterials. Nanotoxicology 9 (7), 871–885. 10.3109/17435390.2014.986670 (Epub 2015/02/13, PubMed PMID: 25672815; PMCID: PMC4782604). [PubMed: 25672815]

Pettibone JM, Adamcakova-Dodd A, Thorne PS, O'Shaughnessy PT, Weydert JA, Grassian VH, 2008 Inflammatory response of mice following inhalation exposure to iron and copper nanoparticles. Nanotoxicology. 2 (4), 189–204. 10.1080/17435390802398291.

Prajapati MV, Adebolu OO, Morrow BM, Cerreta JM, 2017 Original research: evaluation of pulmonary response to inhaled tungsten (IV) oxide nanoparticles in golden Syrian hamsters. Experimental biology and medicine (Maywood, NJ) 242 (1), 29–44. 10.1177/1535370216665173 (Epub 2016/08/19, PubMed PMID: 27534980; PMCID: PMC5206983).

Rossner P Jr., Vrbova K, Strapacova S, Rossnerova A, Ambroz A, Brzicova T, Libalova H, Javorkova E, Kulich P, Vecera Z, Mikuska P, Coufalik P, Krumal K, Capka L, Docekal B, Moravec P, Sery O, Misek I, Fictum P, Fiser K, Machala M, Topinka J, 2018 Inhalation of ZnO nanoparticles: splice junction expression and alternative splicing in mice. Toxicol. Sci. 168 (1), 190–200. 10.1093/toxsci/kfy288.

Saikia J, Yazdimamaghani M, Hadipour Moghaddam SP, Ghandehari H, 2016 Differential protein adsorption and cellular uptake of silica nanoparticles based on size and porosity. ACS Appl. Mater. Interfaces 8 (50), 34820–34832 (Epub 2016/12/06, PubMed PMID: 27998138). [PubMed: 27998138]

Schwotzer D, Ernst H, Schaudien D, Kock H, Pohlmann G, Dasenbrock C, Creutzenberg O, 2017 Effects from a 90-day inhalation toxicity study with cerium oxide and barium sulfate nanoparticles in rats. Part Fibre Toxicol. 14 (1), 23 10.1186/s12989-017-0204-6 (Epub 2017/07/14, PubMed PMID: 28701164; PMCID: PMC5508701). [PubMed: 28701164]

Stopford W, Turner J, Cappellini D, Brock T, 2003 Bioaccessibility testing of cobalt compounds. J. Environ. Monit. 5 (4), 675–680. 10.1039/B302257A. [PubMed: 12948248]

Stueckle TA, Davidson DC, Derk R, Kornberg TG, Schwegler-Berry D, Pirela SV, Deloid G, Demokritou P, Luanpitpong S, Rojanasakul Y, Wang L, 2017 Evaluation of tumorigenic potential of CeO2 and Fe2O3 engineered nanoparticles by a human cell in vitro screening model. NanoImpact 6, 39–54. 10.1016/j.impact.2016.11.001. [PubMed: 28367517]

Sun J, Bostick BC, 2015 Effects of tungstate polymerization on tungsten(VI) adsorption on ferrihydrite. Chem. Geol. 417, 21–31. 10.1016/j.chemgeo.2015.09.015.

Tanaka T, Narazaki M, Kishimoto T, 2014 IL-6 in inflammation, immunity, and disease. Cold Spring Harbor perspectives in biology 6 (10), a016295 10.1101/cshperspect.a016295 (Epub 2014/09/06, PubMed PMID: 25190079; PMCID: PMC4176007). [PubMed: 25190079]

Tedja R, Lim M, Amal R, Marquis C, 2012 Effects of serum adsorption on cellular uptake profile and consequent impact of titanium dioxide nanoparticles on human lung cell lines. ACS Nano 6 (5), 4083–4093. 10.1021/nn3004845. [PubMed: 22515565]

Teoh WY, Amal R, Mädler L, 2010 Flame spray pyrolysis: an enabling technology for nanoparticles design and fabrication. Nanoscale. 2 (8), 1324–1347. 10.1039/C0NR00017E. [PubMed: 20820719]

Toya T, Fukuda K, Takaya M, Arito H, 2001 Lung lesions induced by intratracheal instillation of vanadium pentoxide powder in rats. Ind. Health 39 (1), 8–15. 10.2486/indhealth.39.8 (Epub 2001/02/24, PubMed PMID: 11212290). [PubMed: 11212290]

Vandebriel RJ, De Jong WH, 2012 A review of mammalian toxicity of ZnO nanoparticles. Nanotechnology, science and applications 5, 61–71. 10.2147/nsa.S23932 (Epub 2012/01/01, PubMed PMID: 24198497; PMCID: PMC3781722).

Wang B, Zhang J, Chen C, Xu G, Qin X, Hong Y, Bose DD, Qiu F, Zou Z, 2018 The size of zinc oxide nanoparticles controls its toxicity through impairing autophagic flux in A549 lung epithelial cells. Toxicol. Lett. 285, 51–59. 10.1016/j.toxlet.2017.12.025 (Epub 2018/01/01, PubMed PMID: 29289694). [PubMed: 29289694]

Wells MA, Abid A, Kennedy IM, Barakat AI, 2012 Serum proteins prevent aggregation of Fe2O3 and ZnO nanoparticles. Nanotoxicology 6, 837–846. 10.3109/17435390.2011.625131 (Epub 2011/12/14, PubMed PMID: 22149273; PMCID: PMC3963816). [PubMed: 22149273]

Wiemann M, Vennemann A, Sauer UG, Wiench K, Ma-Hock L, Landsiedel R, 2016 An in vitro alveolar macrophage assay for predicting the short-term inhalation toxicity of nanomaterials. Journal of Nanobiotechnology. 14 (1), 16 10.1186/s12951-016-0164-2. [PubMed: 26944705]

Wolf FI, Cittadini A, 1999 Magnesium in cell proliferation and differentiation. Frontiers in bioscience: a journal and virtual library. 4, D607–D617. 10.2741/wolf (Epub 1999/08/03, PubMed PMID: 10430554). [PubMed: 10430554]

Wongrakpanich A, Mudunkotuwa IA, Geary SM, Morris AS, Mapuskar KA, Spitz DR, Grassian VH, Salem AK, 2016 Size-dependent cytotoxicity of copper oxide nanoparticles in lung epithelial cells. Environ Sci Nano. 3 (2), 365–374. 10.1039/C5EN00271K (Epub 2016/02/24, PubMed PMID: 27347420). [PubMed: 27347420]

Worle-Knirsch JM, Kern K, Schleh C, Adelhelm C, Feldmann C, Krug HF, 2007 Nanoparticulate vanadium oxide potentiated vanadium toxicity in human lung cells. Environmental science & technology. 41 (1), 331–336. 10.1021/es061140x (Epub 2007/02/03, PubMed PMID: 17265967). [PubMed: 17265967]

Xing Z, Bai L, Ma Y, Wang D, Li M, 2018 Mechanism of magnesium oxide hydration based on the multi-rate model. Materials (Basel, Switzerland) 11 (10). 10.3390/ma11101835 (Epub 2018/09/29, PubMed PMID: 30261674; PMCID: PMC6212817).

Zhang J, Qin X, Wang B, Xu G, Qin Z, Wang J, Wu L, Ju X, Bose DD, Qiu F, Zhou H, Zou Z, 2017 Zinc oxide nanoparticles harness autophagy to induce cell death in lung epithelial cells. Cell death & disease 8 (7), e2954 10.1038/cddis.2017.337 (Epub 2017/07/28, PubMed PMID: 28749469; PMCID: PMC5550878). [PubMed: 28749469]

Zhang Z, Zhang R, Xiao H, Bhattacharya K, Bitounis D, Demokritou P, McClements DJ, 2019 Development of a standardized food model for studying the impact of food matrix effects on the gastrointestinal fate and toxicity of ingested nanomaterials. NanoImpact 13, 13–25. 10.1016/j.impact.2018.11.002. [PubMed: 31093583]

Zimmerman JF, Ardoña HAM, Pyrgiotakis G, Dong J, Moudgil B, Demokritou P, Parker KK, 2019 Scatter enhanced phase contrast microscopy for discriminating mechanisms of active nanoparticle transport in living cells. Nano Lett. 19 (2), 793–804. 10.1021/acs.nanolett.8b03903. [PubMed: 30616354]

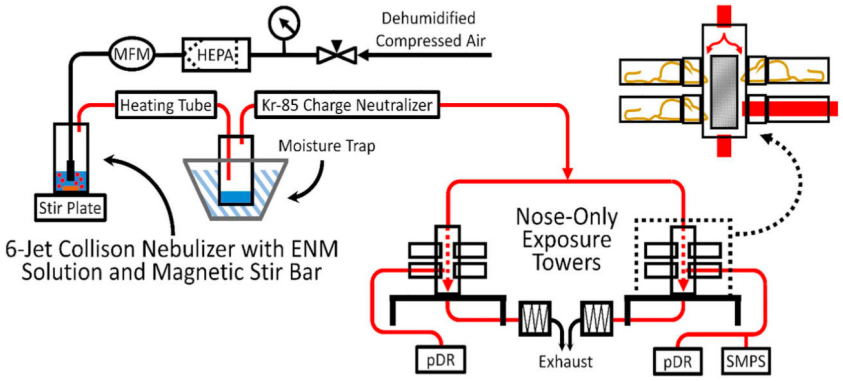

Fig. 1.

Schematic of nanoparticle aerosol generation and nose-only exposure system used in *in vivo* acute studies. ENM suspensions were placed into a 6-jet Collison nebulizer supplied with dehumidified and HEPA-filtered air at 20 psi. Nebulizer-generated aerosol (indicated by red lines) flowed through a heating tube and moisture trap and then passed through a ^{85}Kr charge neutralizer and subsequently entered each nose-only exposure tower at 6 L/min. Size distribution of the ENM aerosol within the exposure towers was evaluated using a SMPS. Real-time ENM aerosol concentration was monitored in each tower using an aerosol photometer (pDR). Time-weighted average ENM aerosol concentrations were determined gravimetrically from pDR filters. The entire system was housed in a chemical hood.

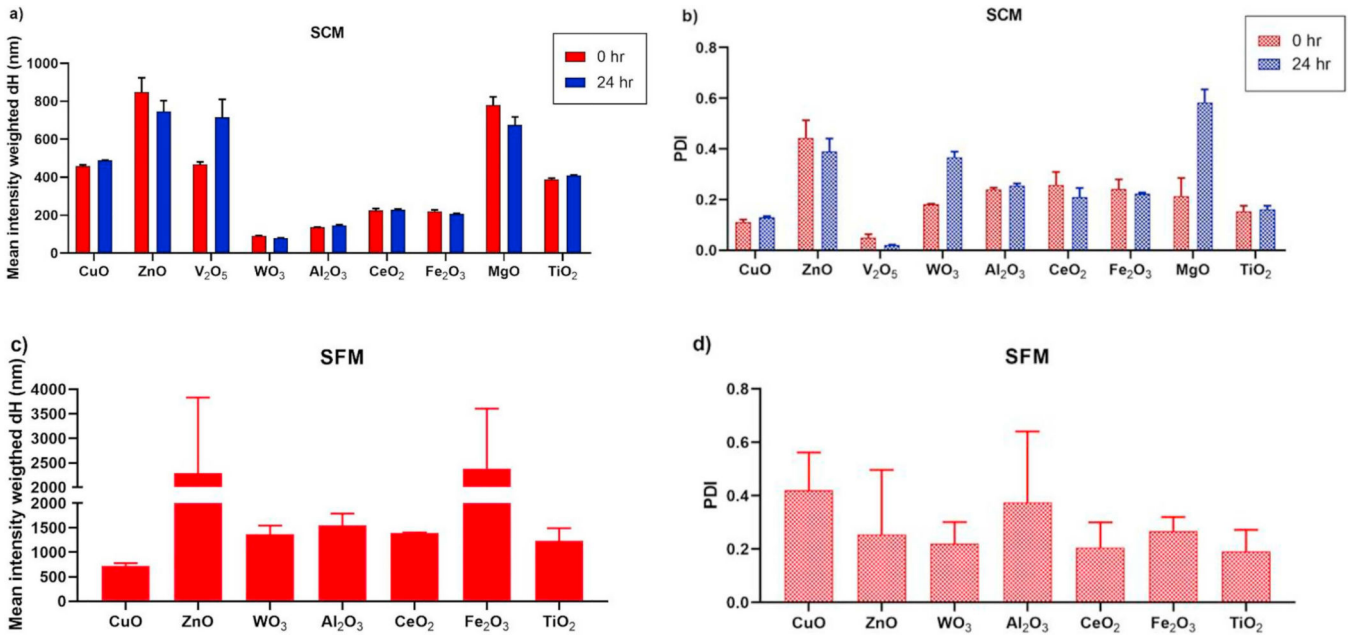

Fig. 2.

(a) Mean intensity weighted hydrodynamic diameter (dH) of ENMs measured at 0 and 24 h incubation in SCM at 37 °C, (b) polydispersity index (PDI) of ENMs measured at 0 and 24 h incubation in SCM, (c) mean intensity weighted dH of ENMs for 0 h incubation, and (d) PDI of ENMs measured at 0 h incubation in SFM.

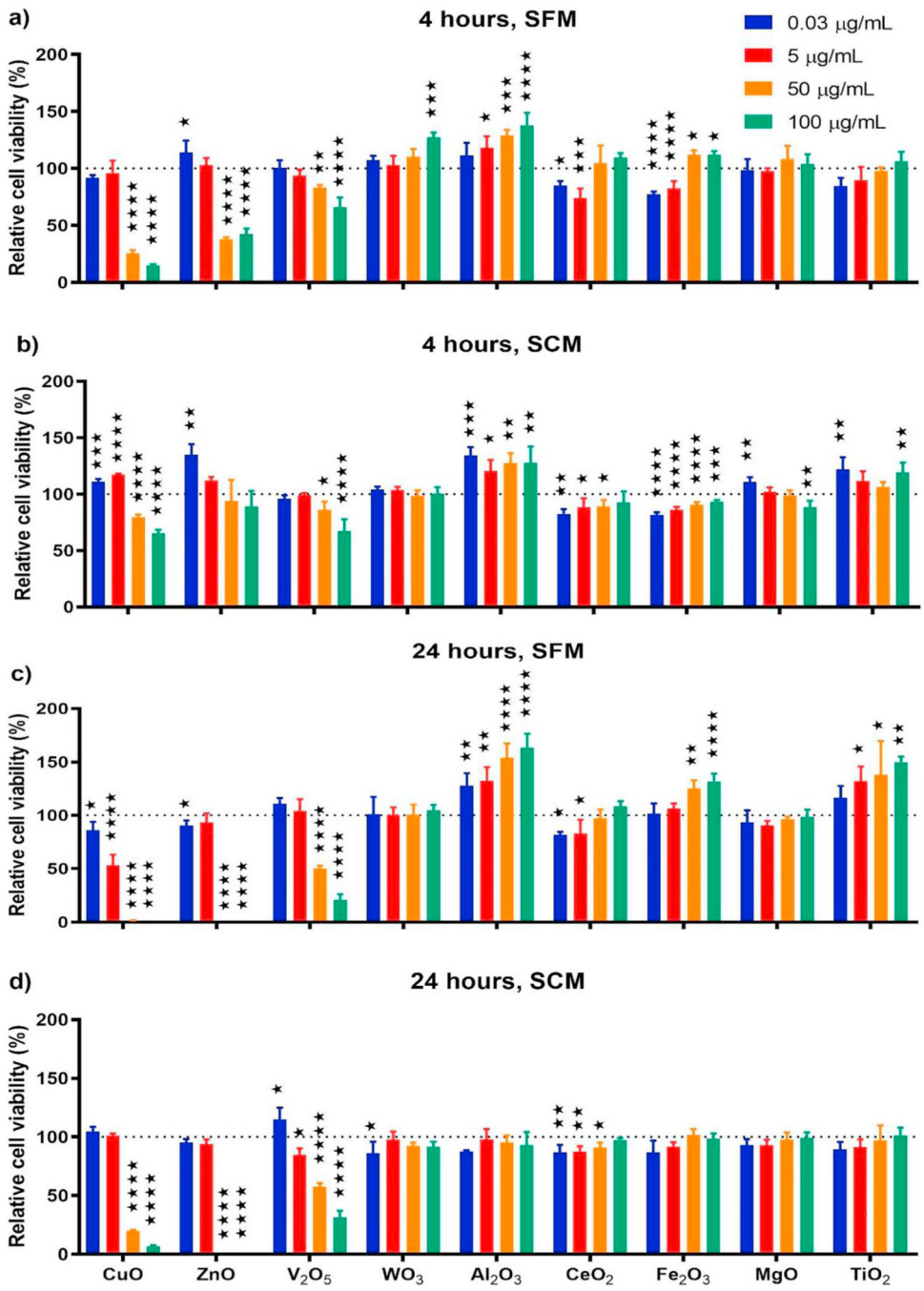

Fig. 3.

Percentage relative cell viability of ENMs at the concentration of 0.03, 5, 50, and 100 μg/mL by MTS assay in (a) SFM for 4 h (b) SCM for 4 h (c) SFM for 24 h and (d) SCM for 24 h.

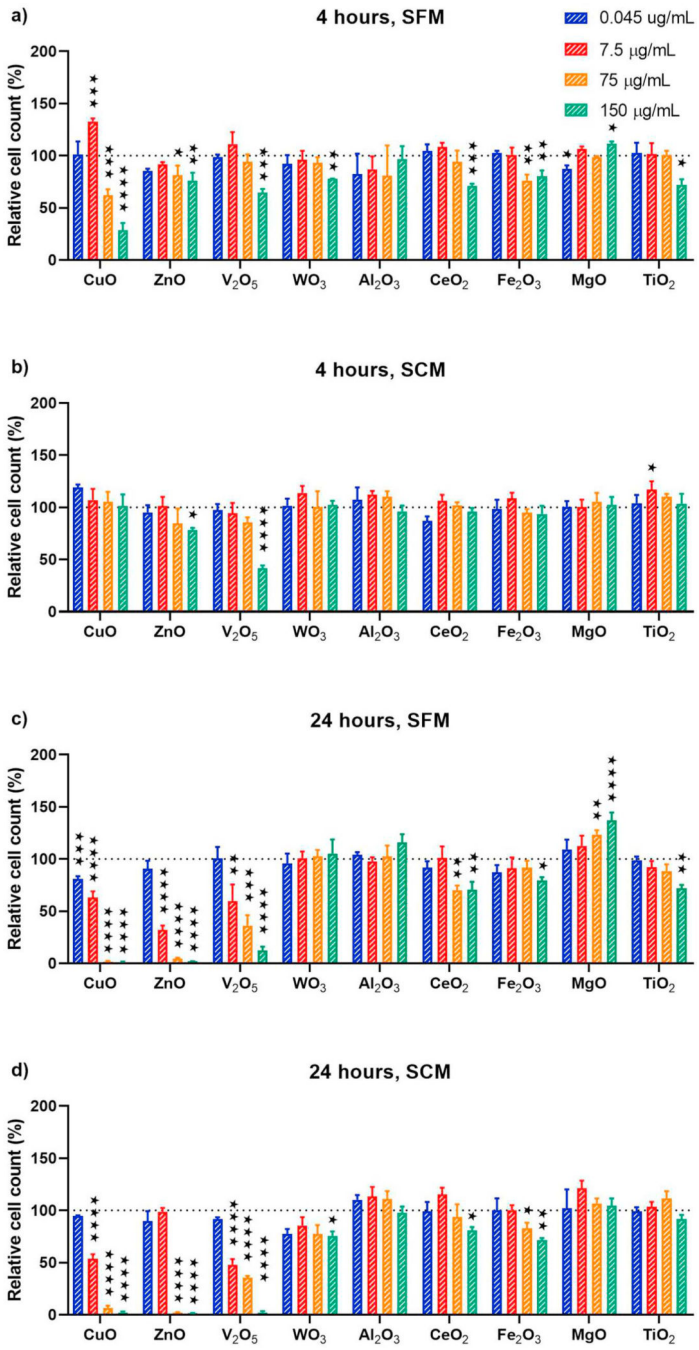

Fig. 4.

Percentage of relative viable cell count of ENMs at the concentration of 0.045, 7.5, 75, and 150 μg/mL using viable cell count with PI staining in (a) SFM for 4 h (b) SCM for 4 h (c) SFM for 24 h and (d) SCM for 24 h.

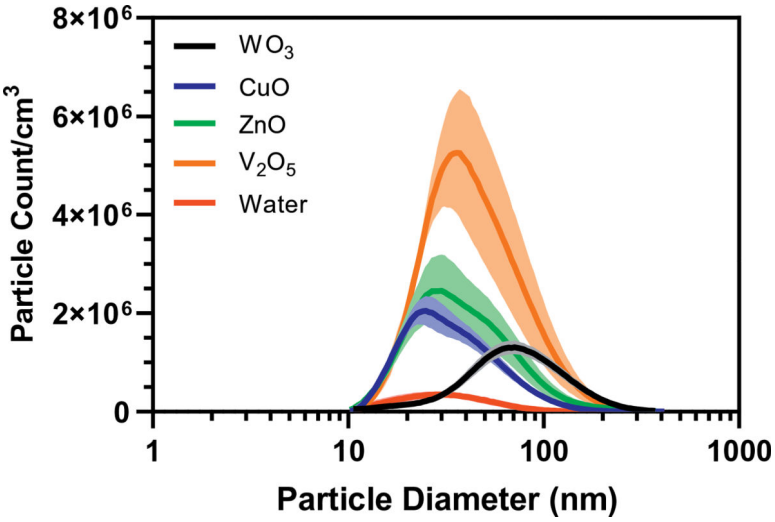

Fig. 5.

Particle size distribution of ENM aerosols generated for nose-only exposures. Measurement was performed using SMPS sampling from the nose-only port of the exposure system.

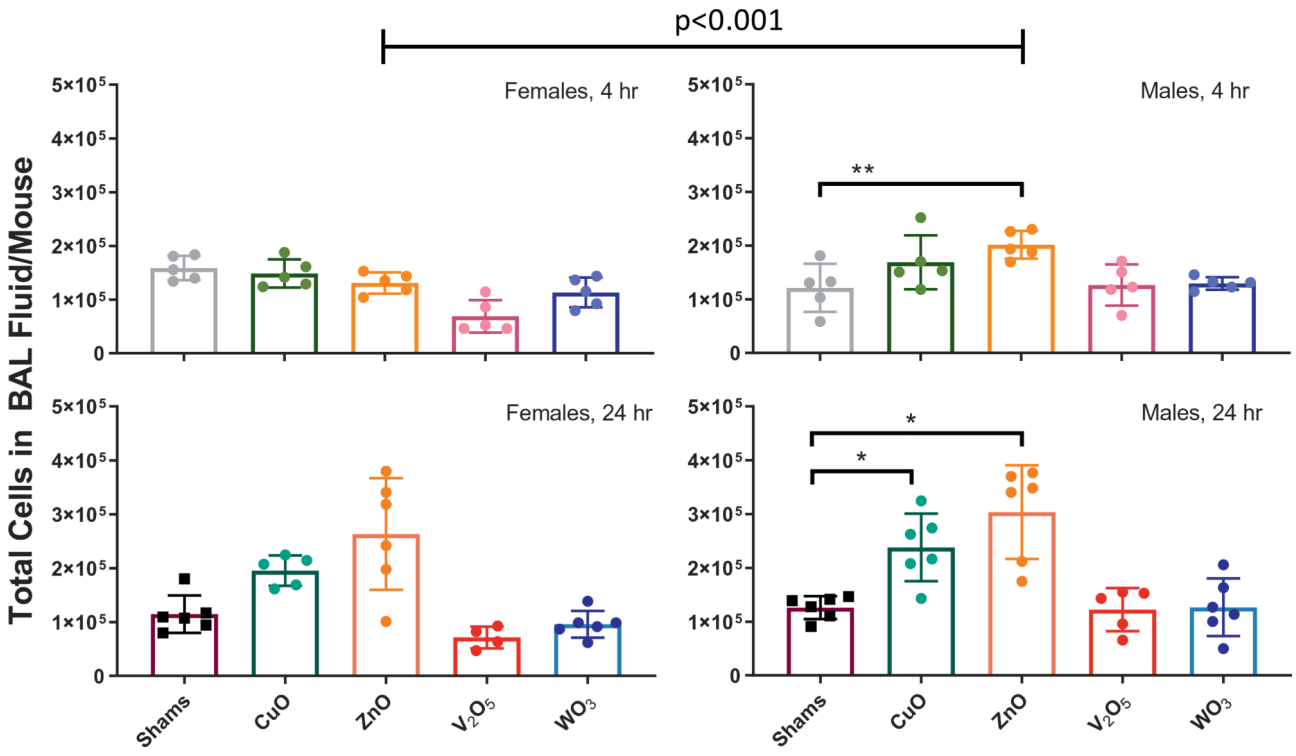

Fig. 6.

Number of total cells in BAL fluid in females and males at 4 h and 24 h time point.

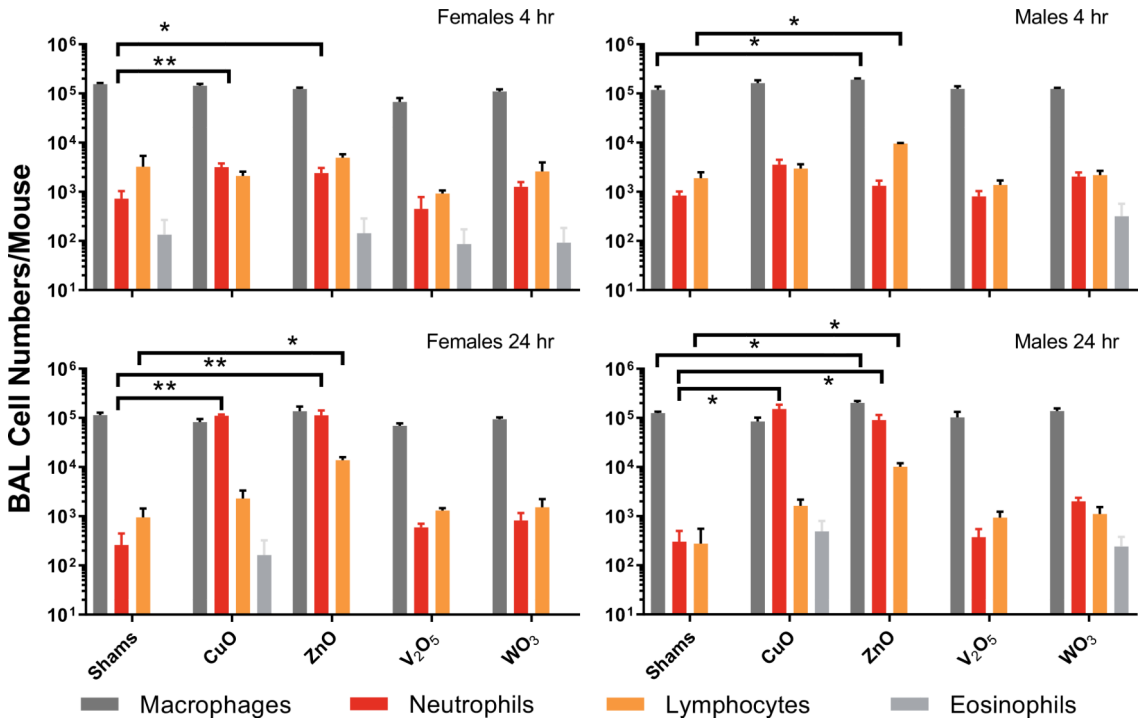

Fig. 7.

Number of macrophages, neutrophils, lymphocytes and eosinophils in BAL fluid in females and males at 4 h and 24 h time point.

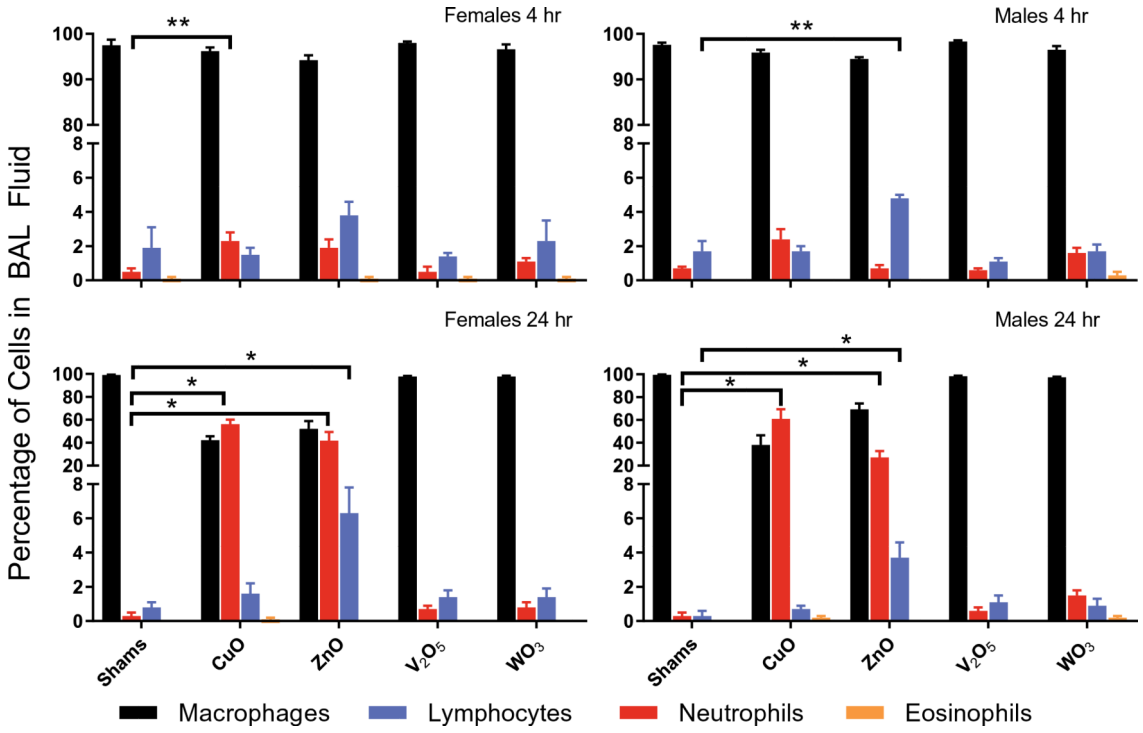

Fig. 8.

Proportion of macrophages, neutrophils, lymphocytes and eosinophils in BAL fluid in females and males at 4 h and 24 h time point.

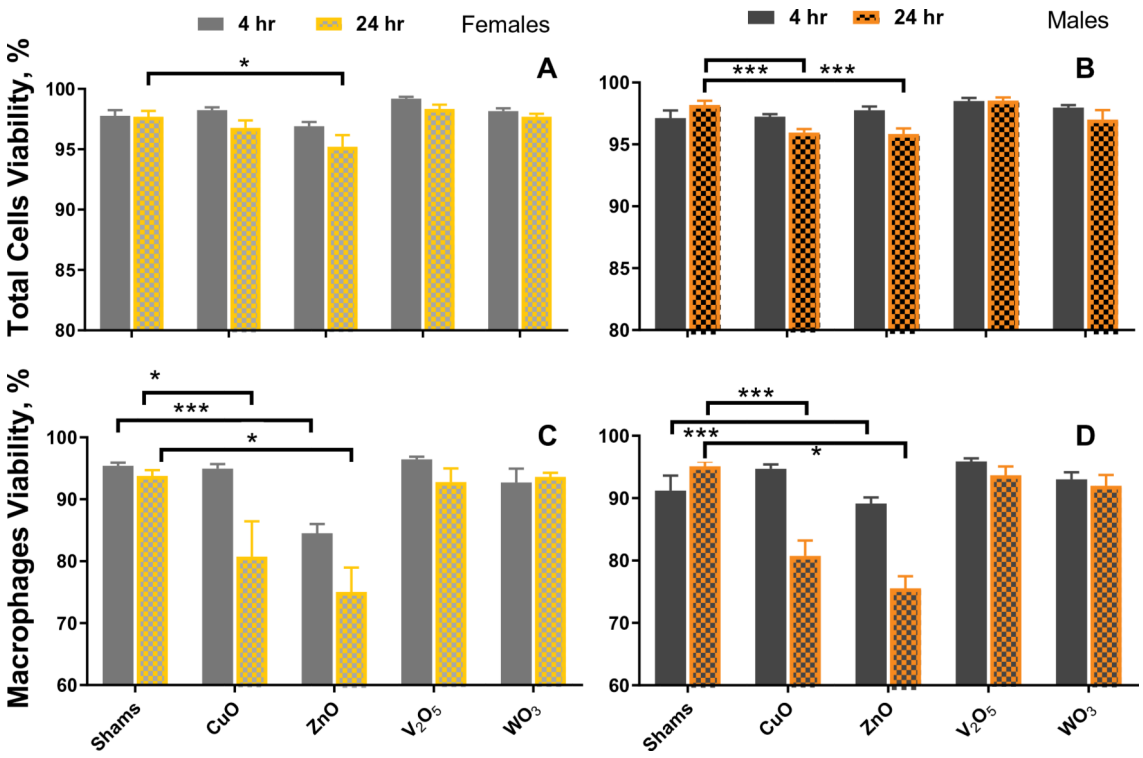

Fig. 9.

BAL cell viability of total cells (A and B) and macrophages (C and D) in females and males at 4 h and 24 h time point.

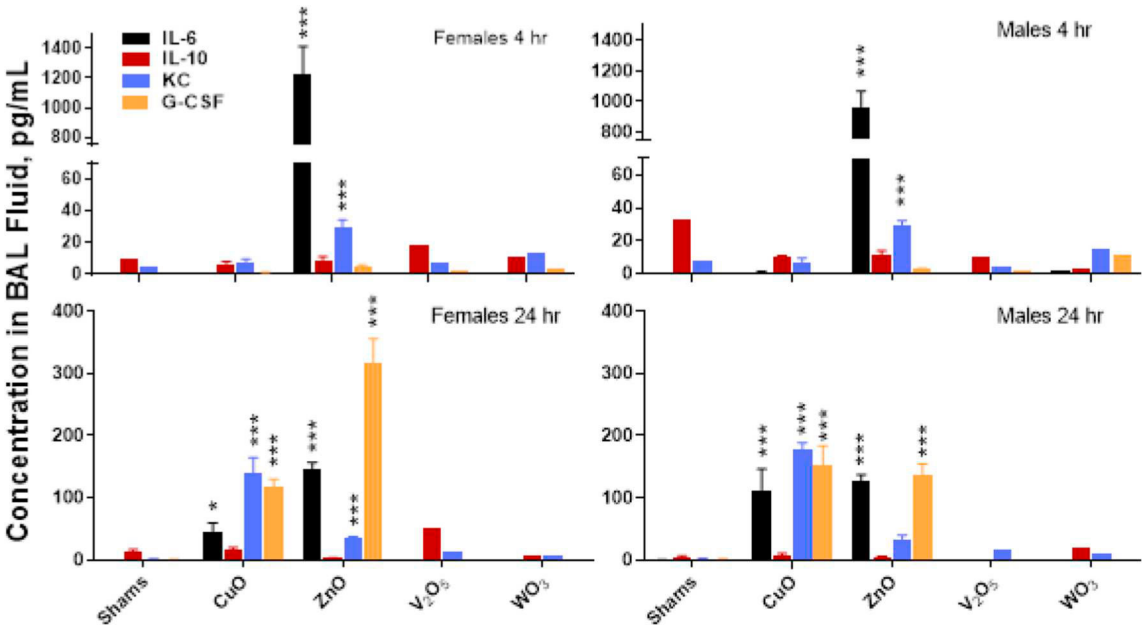

Fig. 10.

Concentration of cytokines in BAL fluid in females and males at 4 h and 24 h time point. Significant differences show difference in comparison with shams.

Table 1

Characterization and dose delivered to cells data of ENMs in SCM.

ENMs	Raw material density (g/cm^3)	Volume-weighted dH (nm)	Effective density (g/cm^3)	Mean fraction of administered ENM deposited for 24 h (unitless)	Mean bottom concentration for 24 h	
					ENM mass per unit volume (mg/mL)	ENM mass per unit area of well (mg/cm^2)
MgO	3.1420 ± 0.0047	852.2 ± 36.3	1.125 ± 0.004	0.3618	54.2718	0.0543
ZnO	6.1547 ± 0.0064	842.6 ± 177.0	1.552 ± 0.111	0.8195	24.5857	0.0246
TiO_2	4.0314 ± 0.0021	569.3 ± 36.2	1.566 ± 0.031	0.4691	14.0720	0.0141
V_2O_5	3.3827 ± 0.0012	467.5 ± 13.28	1.453 ± 0.099	0.2829	8.4867	0.0085
CuO	6.1531 ± 0.0027	418.6 ± 39.2	1.227 ± 0.044	0.1086	0.3258	0.0003
Fe_2O_3	4.4834 ± 0.1540	308.0 ± 27.9	1.226 ± 0.110	0.0313	0.9395	0.0009
CeO_2	7.5314 ± 0.0173	268.4 ± 20.9	1.774 ± 0.030	0.1370	4.1114	0.0041
Al_2O_3	3.5939 ± 0.0391	186.8 ± 5.3	1.943 ± 0.190	0.0629	1.8884	0.0019
WO_3	7.6659 ± 0.0272	82.3 ± 2.4	1.588 ± 0.370	0.0047	0.1426	0.0001

Table 2

Exposure concentrations and particle size distributions of generated aerosol for *in vivo* studies.

Type of ENMs	Concentration of NPs used in Collison nebulizer[b]	Exposure aerosol concentration, mg/m^3		Aerosol size distribution, GM, nm (GSD)[a]	Peak particle count/cm^3
		Toxicity evaluation	Dosimetry assessment		
ZnO	0.3 mg/mL	3.75	3.80	37.5 (1.78)	2.46×10^6
CuO	1 mg/mL	3.77	3.61	33.3 (1.70)	2.05×10^6
V_2O_5	1 mg/mL	4.15	4.19	43.0 (1.71)	5.26×10^6
WO_3	0.4 mg/mL	3.24	2.95	77.6 (1.72)	1.37×10^6

[a] Geometric mean mobility diameter (GM) with geometric standard deviation (GSD).

[b] The pressure and air flow through 6-jet Collison Nebulizer was the same for all ENMs evaluated: 20 psi and 12 L/min, respectively.

Table 3

Estimated exposure doses for acute nose-only exposure.

ENM	Deposition fraction in pulmonary region	Estimated dose[a]			
		By mass mg/kg	By animal μg/mouse	By lung mass μg/g[c]	By lung surface[b] ng/cm^2
ZnO	0.21	0.23	4.7	39.0	6.9
CuO	0.22	0.25	4.9	41.1	7.2
V_2O_5	0.20	0.25	4.9	41.1	7.2
WO_3	0.14	0.14	2.8	22.5	4.1

[a] Assumes 165 breaths/min, tidal volume of 0.15 mL, and 20 g/mouse body mass.

[b] 680 cm^2 surface area.

[c] Wet weight of whole lungs used in this estimation was 120 mg.

Table 4

Concentration of selected isotopes in lung tissues of exposed and control animals at 4 and 24 h post exposure, determined by ICP-MS. Data were adjusted for digestion efficiency.

Investigated ENM	Measured isotope	Concentration, μg/g (dry wt) Mean ± SE		
		Shams (n = 5)	4 h (n = 5)	24 h (n = 5)
CuO	^{63}Cu	12.1 ± 0.8	60.0 ± 1.6 ***	50.9 ± 2.1 ***
ZnO	^{64}Zn	196.1 ± 6.0	181.1 ± 20.9	116.7 ± 1.1
V_2O_5	^{51}V	0.3 ± 0.0	31.8 ± 2.6 ***	18.2 ± 0.8 *
WO_3	^{183}W	0.2 ± 0.0	58.6 ± 4.8 ***	19.8 ± 2.1 ***

* $p < 0.05$

*** $p < 0.001$ significantly higher from shams.